Geochemistry Geophysics Geosystems G3
AN ELECTRONIC JOURNAL OF THE EARTH SCIENCES
Published by AGU and the Geochemical Society

*Article*
Volume 2
September 4, 2001
Paper number 2000GC000132
ISSN: 1525-2027

# Petrogenesis of the crust-mantle transition zone and the origin of lower crustal wehrlite in the Oman ophiolite

**Kenneth T. Koga, Peter B. Kelemen, and Nobumichi Shimizu**

Woods Hole Oceanographic Institution, M. S. 23, Woods Hole, Massachusetts 02543-1541, USA
(ktkoga@misasa.okayama-u.ac.jp; pkelemen@whoi.edu; nshimizu@whoi.edu)

[1] **Abstract:** We studied trace element geochemistry and petrology of the crust-mantle transition zone (MTZ) in the Samail massif of the Oman ophiolite to constrain the location where different primitive magmas mix beneath an oceanic spreading ridge. The MTZ is the deepest location where crystallization took place and thus is an ideal place to determine the compositional diversity of melts leaving the mantle, with various sources and degrees of depletion. We have reached three main conclusions: (1) More than 90% of our samples record equilibration with compositionally indistinguishable parental melts, similar to mid-ocean ridge basalts (MORB) and the melts that formed the crust in Oman. This suggests that mixing of diverse, polybaric partial melts of mantle peridotite occurred at or below the depth of the MTZ. The presence of distinct heterogeneity in less than 10% of our samples is similar to the nature and frequency of heterogeneity observed in melt inclusions in olivines from MORB. (2) Among the samples recording trace element equilibrium with MORB-like liquids are wehrlitic rocks, previously suggested to be cumulates from an unusual parental melt on the basis of petrological observation. (3) Systematics of Eu distribution among plagioclase and clinopyroxene in "impregnated peridotites" demonstrate that these minerals did not crystallize from "trapped melt." As a consequence, it is not possible to use the modal proportion or texture of plagioclase + clinopyroxene impregnations to estimate the instantaneous melt porosity or the shape of melt pores at any time during the formation of these rocks.

**Keywords:** ophiolite; wehrlite; oceanic crust; rare earth elements; clinopyroxene; Oman.

**Index terms:** Mid-ocean ridge processes; igneous petrology; minor and trace element compositions; major element compositions.

**Received** December 6, 2000; **Revised** June 10, 2001; **Accepted** June 19, 2001; **Published** September 4, 2001.

Koga, K. T., P. B. Kelemen, and N. Shizumu, 2001. Petrogenesis of the crust-mantle transition zone and the origin of lower crustal wehrlite in the Oman ophiolite, *Geochem. Geophys. Geosyst.*, vol. 2, Paper number 2000GC000132 [17,079 words, 8 figures, 8 tables]. Published September 4, 2001.

## 1. Introduction

[2] Recent studies of mid-ocean ridge basalt (MORB) generation suggest that MORB represents a mixture of distinct melts from various upper mantle depths and degrees of melting, which may be produced by a near-fractional melting process [e.g., *Johnson et al.*, 1990;

*Klein and Langmuir*, 1987]. Indeed, *Kinzler and Grove* [1992a] used a parameterization based on their experimental results to show that no individual melt from any specific depths is similar to MORB, and instead inferred that MORB must be a mixture of polybaric partial melts. The presence of heterogeneous melt inclusions in olivines from MORB [e.g., *Shimizu and Hassler*, 1993; *Sobolev and Shimizu*, 1993] shows that variable compositions of mantle-derived melts do reach lower crustal depths, so that the mixing of different melts is not always complete. However, in general, MORB compositions are less variable than those predicted for polybaric melts, and less variable than those observed in melt inclusions. Thus heterogeneous, polybaric melts must mix at some level prior to eruption.

[3] Three possible mixing scenarios for polybaric, mantle-derived melts are considered in this paper. (1) Aggregation of polybaric melts may occur at the base of the lithosphere because of accumulation of melt beneath a porosity barrier at the base of the conductive boundary layer e.g., *Sparks and Parmentier*, 1991; *Spiegelman*, 1993; *Kelemen and Aharonov*, 1998]. Geophysical observations at the East Pacific Rise support the hypothesis that melt accumulates at the base of the crust [*Crawford et al.*, 1999; *Dunn and Toomey*, 1997; *Garmany*, 1989]. (2) Aggregation of polybaric melts may occur in a shallow magma chamber (1–2 km below the ocean floor) consistently observed beneath fast-spreading ridges [*Detrick et al.*, 1987; *Kent et al.*, 1990; *Sinton and Detrick*, 1992]. (3) Mixing may occur during transport of polybaric melts through melt conduits in the melting region [e.g., *Kelemen et al.*, 1997a, 2000; *Spiegelman et al.*, 2001; *Nicolas*, 1986; *Prinzhofer and Allegre*, 1985]. This study was designed to test the hypothesis that mixing of polybaric melts occurs mainly at or beneath the crust-mantle transition zone.

[4] The crust-mantle transition zone (MTZ) in the Oman ophiolite represents a zone where ascending melt begins to crystallize to form the crust and provides an ideal locale for investigating the diversity of melt composition passing from the mantle into the crust. This paper describes geochemical and petrological observations made on samples from the well-studied MTZ in the Maqsad region of the Samail massif in the Oman ophiolite [e.g., *Jousselin et al.*, 1998; *Boudier and Nicolas*, 1995; *Ceuleneer et al.*, 1988; *Nicolas et al.*, 1988a]. The Oman ophiolite is considered to be a good example of a medium- to fast-spreading ridge [*Nicolas et al.*, 2000a; *Nicolas*, 1989; *Tilton et al.*, 1981], and ages of tectonic events are well documented [e.g., *Tilton et al.*, 1981; *Coleman*, 1981; *Hacker*, 1994]. The MTZ in the Oman ophiolite is composed of diverse rock types. This study focuses on the possible diversity of parental melt compositions and their implications for MORB petrogenesis. We report major and trace element contents of minerals, mainly clinopyroxene, in samples from the MTZ. Trace element contents of "cumulate" clinopyroxene are used to infer the composition of melts which passed from the mantle into the overlying crust. Most samples record equilibration with a homogeneous, primitive melt, similar in trace element abundance to the melts that formed overlying gabbros and volcanic rocks. Two of 23 samples from the Maqsad area are compositionally distinct and are interpreted to record incomplete mixing of melts at and below the MTZ. The rare occurrence of such samples suggests that the volume of unmixed melts was small. Therefore we infer that the mixing processes to form parental MORB must have occurred mainly within the mantle, at depths greater than the MTZ.

[5] In addition to this main conclusion our data can also be used to constrain petrogenesis of specific MTZ lithologies. Much emphasis has been placed on the presence of wehrlitic rocks,

whose apparent sequence of crystallization (olivine followed by clinopyroxene, then followed by plagioclase) is different from the more abundant gabbroic rocks (olivine-plagioclase-clinopyroxene). Some previous workers have suggested that the wehrlitic rocks formed by crystallization of a mantle-derived melt composition that was significantly different from the melt that formed the gabbroic rocks [e.g., *Pallister and Hopson*, 1981; *Smewing*, 1981; *Juteau et al.*, 1988], whereas others have proposed that they formed via Moho-level interaction of MORB-like melts with residual peridotites [e.g., *Boudier and Nicolas*, 1995] and/or seawater. Our trace element data on clinopyroxene in the wehrlitic rocks are indistinguishable from data on clinopyroxene in gabbroic rocks and suggest that the wehrlitic rocks did not form from a compositionally distinct primary melt.

[6] Many recent papers have relied on textural data from "impregnated peridotites," residual peridotites, and dunites which include later, igneous plagioclase and clinopyroxene precipitated from a melt to make inferences about the porous melt fraction and shape of melt pores in the shallow mantle beneath mid-ocean ridges [e.g., *Jousselin and Mainprice*, 1998; *Jousselin et al.*, 1998]. Our data show that the plagioclase and clinopyroxene in Oman "impregnated peridotites" crystallized in an open system, from which melt was subsequently removed. As a result, the proportion and shape of plagioclase and clinopyroxene in these rocks cannot be used to estimate the melt fraction and shape of melt pores at any time during the formation of these rocks.

## 2. Geology

[7] The Oman ophiolite massifs extend ~500 km in a NW-SE direction along the northern coastline of the Sultanate of Oman (Figure 1), representing oceanic crust and upper mantle that was obducted during the closure of the Tethys ocean 90 million years ago [*Coleman*, 1981; *Hacker*, 1994]. Many of the massifs, including the Samail massif studied here, preserve complete ophiolite sequences, including pillow basalts, sheeted dikes, cumulate gabbros, and mantle peridotites [e.g., *Nicolas*, 1989]. The MTZ lies above the uppermost mantle harzburgites and below the top contact of the uppermost massive dunites (more than 10 m thick), below massive layered gabbro of the lower crust [*Benn et al.*, 1988]. The MTZ consists mainly of dunite, troctolite, gabbro, and wehrlite [e.g., *Boudier and Nicolas*, 1995; *Nicolas and Prinzhofer*, 1983]. Below the MTZ there is often a zone of diffuse "impregnated peridotite," with interstitial plagioclase and clinopyroxene within deformed harzburgite, interpreted as the products of partial crystallization of cooling melts migrating by porous flow through residual mantle harzburgite [e.g., *Ceuleneer and Rabinowicz*, 1992]. In the Maqsad area of the Samail massif in the southern Oman Mountains the base of the lower crustal gabbros is nearly horizontal and lies above a thick (~500 m) MTZ section exposed by erosion [e.g., *Boudier and Nicolas*, 1995]. In addition to 23 samples from the Maqsad area, four wehrlite samples were collected from Wadi Aqsaybah, in the Wadi Tayin massif, where wehrlitic bodies, including true wehrlite, intrude lower crustal layered gabbros [*Pallister and Hopson*, 1981].

[8] Dunite and gabbro are the most abundant constituents of the MTZ, and they are commonly interlayered. The layering is parallel to the base of the lower crustal layered gabbros. Both diffuse and sharp contacts are observed between dunite and gabbro. The diffuse contacts show intergranular plagioclase and/or pyroxene between olivine crystals in dunite. Chilled margins are not observed at diffuse or sharp contacts. In the Maqsad area, gabbros exist as sills or lenses parallel to the base of the

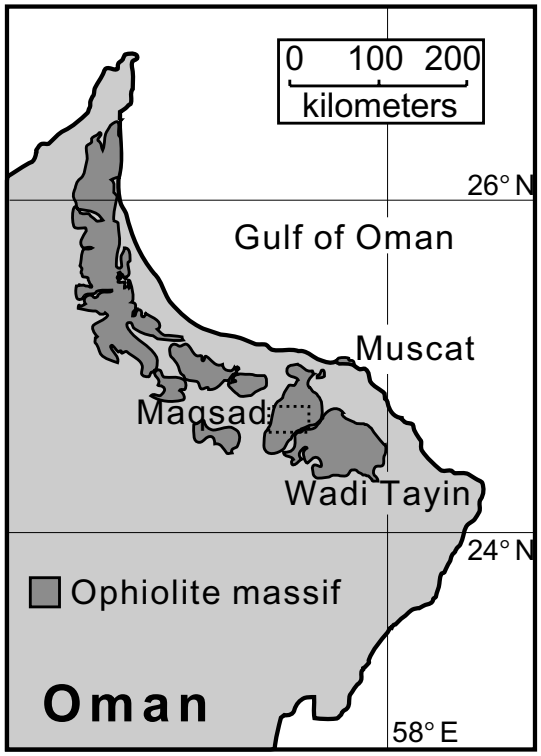


**Figure 1.** Map showing the location of the Oman ophiolite massifs (dark gray regions). A dotted rectangle indicates the area of Figure 2.

lower crustal gabbros. Gabbro sill thicknesses vary from a few meters to tens of meters, while their lengths vary from a few meters to more than 100 meters along strike. The occurrence of sills increases toward the base of the lower crustal gabbros. Dunites are massive and surround gabbro sills. Dunite thicknesses between gabbro sills also vary from a few centimeters to many tens or even hundreds of meters, and the thickness and proportion of dunites decreases toward the base of the lower crustal gabbros [*Boudier and Nicolas*, 1995]. Discordant gabbronorite dikes crosscut all lithologies from mantle harzburgite to lower gabbro, and some of these show distinct chilled margins. Because of the crosscutting relationship and the chilled margins, both of which suggest a significantly later, off-axis origin for the gabbronorite dikes, we did not include them among MTZ samples discussed in this paper.

[9] In this study, we have tried to describe rocks in a way that is consistent with both petrological classification and with the mapping terms that have been used in the field in the past [e.g., *Nicolas*, 1986]. This is especially important for wehrlitic rocks, since the term "wehrlite" has been used in the past as a map unit including a range of clinopyroxene(cpx)-olivine-rich rocks showing characteristic field relations.

[10] The term "gabbro" refers to rocks with more than 10% plagioclase, more than 10% clinopyroxene, and less than 5% orthopyroxene. An olivine gabbro has more than 5% olivine. In Oman, some troctolites (>95% plagioclase + olivine and <5% clinopyroxene) and a few gabbronorites have been mapped as "gabbro," while many true gabbros and troctolites have been mapped as "wehrlite." In this paper, gabbro, troctolite, and olivine gabbro with more than 30% plagioclase will be referred to as "gabbroic rocks." In the Oman MTZ the gabbroic rocks are layered sills that are distinctly different in their plagioclase content from surrounding dunitic rocks. Unlike dunitic rocks, all gabbro sill samples have modal layering and a mosaic microstructure. They are also commonly altered, with up to ~30 vol % hydrous, secondary phases.

[11] The term "dunite" refers to rocks with >90% olivine (and alteration phases replacing olivine). In Oman some olivine-rich troctolites and clinopyroxene-poor, olivine-rich gabbros have been mapped as "impregnated dunite," and these are grouped with true dunites in this paper under the term "dunitic rocks." Most of the dunitic rocks in the MTZ are impregnated to some extent, but there are also some true dunites showing little or no impregnation (e.g., OM94-34, OM94-39). All dunitic rocks are more than ~60 vol % serpentinized. Dunitic

rocks usually consist of elongated (aspect ratio of 1:~2–3) olivine with a maximum grain width around 1 mm, a few percent subhedral spinel crystals around 200 μm in diameter, and trace amounts of plagioclase and pyroxene where they are impregnated.

[12] Strictly speaking, the term "wehrlite" should refer to rocks with more than 40% olivine and 50% clinopyroxene (and alteration phases replacing olivine and clinopyroxene). In practice, the term "wehrlite" has often been applied in Oman as a field term for dark-colored, plagioclase-poor olivine gabbro (melagabbro). In this paper, we will use the term "true wehrlite" to refer to rocks with more than 40% olivine and 50% clinopyroxene, the term "melagabbro" to refer to olivine gabbros with 10–30% plagioclase (and alteration phases replacing plagioclase), and the term "wehrlitic rocks" to refer to both melagabbro and true wehrlite. Wehrlitic rocks are observed as concordant sills or lenses and also as intrusions crosscutting gabbro and dunite in the MTZ and lower crustal layered gabbro [e.g., *Juteau et al.*, 1988] but never crosscutting residual mantle harzburgites below the MTZ [*Pallister and Hopson*, 1981]. Wehrlitic rocks analyzed in this study were mainly from the Maqsad MTZ, but in addition, we analyzed samples from a wehrlitic intrusion cutting crustal gabbros in Wadi Aqsaybah [*Pallister and Hopson*, 1981].

[13] Most wehrlitic rocks in Oman include some plagioclase oikocrysts e.g., *Juteau et al.*, 1988]. True wehrlites are rare, but do occur (e.g., Figure 3n of *Pallister and Hopson* [1981]). Their presence suggests that some primary magmas beneath the Oman spreading ridge, perhaps parental to all the wehrlitic rocks, had the crystallization sequence olivine-clinopyroxene-plagioclase. If so, these represent compositionally distinct parental melts, because Oman troctolites and genetically related olivine gabbros record the crystallization sequence olivine-plagioclase-clinopyroxene, typical of MORB crystallization at crustal pressures. Thus the occurrence of wehrlitic rocks in the lower crust and the MTZ has been interpreted as evidence for the existence of a melt distinctly different from MORB, such as a picritic liquid [*Ernewein et al.*, 1988; *Juteau et al.*, 1988].

## 3. Analytical Methods

[14] Sample locations were recorded using a portable Global Positioning System within an error of ±100 m (Figure 2 and Table 1). When samples were banded (or layered), thin sections were cut perpendicular to the layering. Modal proportions of minerals in each sample were measured by point counting on 2 by 4 inch thin sections, with an error analysis based on the formulation of *Solomon* [1963]. The grid spacing was chosen on the basis of the size of the smallest crystals of interest in order to avoid aliasing. Counts were accumulated until a statistically significant number of data were collected. The final coverage of counted areas thus varies from sample to sample. In estimating the igneous mode of the rock, the areas occupied by various alteration phases were assigned to their parental minerals on the basis of petrographic interpretation.

[15] Major element compositions in minerals were measured using an electron microprobe (JEOL 733 superprobe at Massachusetts Institute of Technology (MIT)). Operating conditions were as follows: 15 kV accelerating voltage, ~10 nA beam current, and 10 μm beam diameter, using programmed matrix corrections [*Albee and Ray*, 1970; *Bence and Albee*, 1968]. Na is measured at the beginning of each analysis to minimize Na migration. Major element analyses were made on all igneous mineral phases that remained unaltered in the rock. Detailed analyses of clinopyroxene

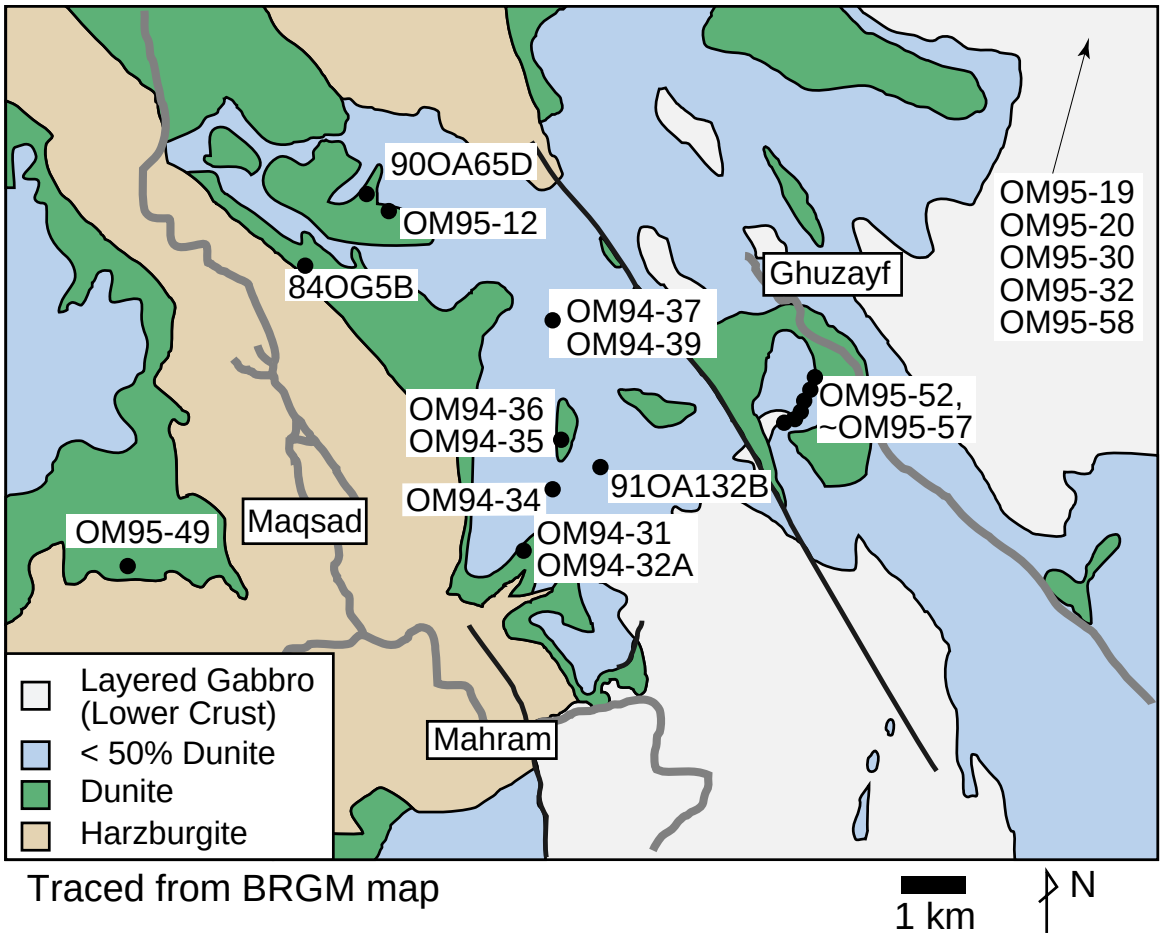


**Figure 2.** Simplified geologic map of the Maqsad area of the Samail massif, southern Oman ophiolite, based on geologic maps made by the French Bureau de Recherches Géologiques et Minières (BRGM) and published by the Sultanate of Oman. The green region indicates the part of the crust-mantle transition zone, or MTZ, with predominantly dunitic rocks. The light blue region indicates the part of the MTZ with a mixture of gabbroic and dunitic rocks. Layered gabbro (i.e., lower crust) is shown by the off-white region. Residual mantle harzburgite is shown as the tan region. The locations of samples analyzed for this study are indicated with solid circles and sample numbers. Light gray lines are roads. Thick black lines are major faults.

were made in the vicinity of ion probe analysis points. At least one compositional traverse across a crystal was determined for each mineral in each sample to determine the nature of possible zoning. The variability of mineral composition in each sample was assessed via multiple measurements on several crystals in each sample. When a mineral phase was zoned, core and rim compositions are reported as the average of core and rim analyses, respectively.

[16] Trace element compositions in clinopyroxene were measured using the secondary ion mass spectrometer (Cameca IMS3f at Woods Hole Oceanographic Institution). Trace element abundance was determined by the energy-filtering techniques described by *Shimizu and Hart* [1982], with a 20 eV energy window and a −90 V energy offset from a 4500 V secondary accelerating voltage, a five-cycle routine in which each cycle used a 20 s counting time

**Table 1.** Sample Catalog

| Sample | Massif | Type | Longitude–Latitude | Outcrop | Local Description | Rock Description | Orientation | Outcrop Description | Thin Section Observation |
|---|---|---|---|---|---|---|---|---|---|
| 84OG5B | Ibra/Samail | troctolite | 23°6.00′N, 57°57.15′E | | tuff | | | | elongated olivne (1:3), reacted rim strongly oriented; plagioclase is heavily altered though aligned parallel to olivine elongation; cpx is worm-like shape around olivine, serpentinized, hydrothermal reaction |
| 90OA65D | Ibra/Samail | plagioclase wehrlite | 23°6.36′N, 57°57.55′E | | tuff | | | | elongated olivine (1:3), serpentinized; spinel is in grain boundaries, in serpentine; cpx has two appearances, large (∼1600 m) and grain boundary, worm-like (width of ∼30 m) |
| 91OA132B | Ibra/Samail | gabbro | 23°3.98′N, 58°0.09′E | | Wadi Qawasim, a branch | | | | large grains (1–2 mm); olivine is not deformed |
| OM94-31 | Ibra/Samail | dunite | 23°3.34′N, 57°59.71′E | near 94MA-1 | Wadi Qawasim. 0.5 km upstream from MA-1 | dunite with wehrlite intrusion | | | olivine is weakly elongated (<1:2); plagioclase and cpx are poikiloblastic, include olivine; large area of poikilitic plagioclase and cpx extinct together |
| OM94-32A | Ibra/Samail | gabbro | 23°3.34′N, 57°59.71′E | near A-1 | Wadi Qawasim. 0.5 km upstream from MA-1 | mixed zoned, layered gabbro | | | olivine is elongated (1:3), banded serpentinized; cpx is interstitial in between olivine and plagioclase, intercumulate texture (long, ∼30 m width); cpx in olivine banding is subhedral up to 1 mm, intercumulus |

**Table 1.** (continued)

| Sample | Massif | Type | Longitude–Latitude | Outcrop | Local Description | Rock Description | Orientation | Outcrop Description | Thin Section Observation |
|---|---|---|---|---|---|---|---|---|---|
| OM94-34 | Ibra/Samail | dunite | 23°3.7′N, 58°0.0′E | 94MA-2 | Wadi Qawasim | dry dunite with low-angle foliation | | | olivine is weakly elongated, oriented; spinel is euhedral surrounded by serpentine; cpx is interstitial |
| OM94-35 | Ibra/Samail | dunite | 23°4.3′N, 57°59.9′E | 94MA-3 | Wadi Qawasim | "protosills" gabbro in dunite | horizontal dunite layer, gabbro dike (305°, 80°SW dip) | dunite containing many cpx veins; there are also horizontal microgabbro dikes and semihorizontal gabbroic impregnation; cpx impregnation shows plastic eformation, but only 15 cm above, there are dunite and gabbro veins; there also are toroctlitic patches in dunite and no transposition; it is likely that dunite is at early foliation stage | olivine is elongated (1:2∼3) and subparallel to banding of impregnations as well as orientation of crystal, serpentinized; plagioclase and cpx are poikiloblastic, and large area extinct at once |
| OM94-36 | Ibra/Samail | dunite | 23°4.3′N, 57°59.9′E | 94MA-3 | Wadi Qawasim, 30 m north of OM94-35 | pyroxenite impregnation in dunite, wehrlitic dunite | gabbro dike (285°, 67°N) | dunite containing mainly cpx veins; there are also horizontal microgabbro dikes and semihorizontal gabbroic impregnation; cpx impregnation shows plastic deformation, but only 15 cm above, there are dunite and gabbro veins; there also are toroctlitic patches in dunite and no transposition; it is likely that dunite is at early foliation stage | olivine is serpentinized, oriented; plagioclase is changing to clay; cpx and clayish plagioclase show poikilitic texture |

**Table 1.** (continued)

| Sample | Massif | Type | Longitude–Latitude | Outcrop | Local Description | Rock Description | Orientation | Outcrop Description | Thin Section Observation |
|---|---|---|---|---|---|---|---|---|---|
| OM94-37 | Ibra/Samail | dunite | 23°5.2′N, 57°59.8′E | 94MA-5 | Wadi Qawasim, near ridge crest | dunite with intercumulus | | dunite containing mainly cpx veins; there are also horizontal microgabbro dikes and semihorizontal gabbroic impregnation; cpx impregnation shows plastic deformation, but only 15 cm above, there are dunite and gabbro veins; there also are toroctlitic patches in dunite and no transposition; it is likely that dunite is at early foliation stage | olivine is well oriented, weakly elongated; amphiboles are replacing plagioclase and cpx; cpx shows worm-like intergranular texture |
| OM94-38 | Ibra/Samail | dunite | 23°5.2′N, 57°59.8′E | 94MA-5 | Wadi Qawasim, near ridge crest | dunite host of OM94-38 | | dunite containing mainly cpx veins; there are also horizontal microgabbro dikes and semihorizontal gabbroic impregnation; cpx impregnation shows plastic deformation, but only 15 cm above, there are dunite and gabbro veins; there also are toroctlitic patches in dunite and no transposition; it is likely that dunite is at early foliation stage | elongated olivine (1:2), 1–2 mm size; spinel is abundant; no cpx |
| OM94-39 | Ibra/Samail | dunite | 23°5.34′N, 57°59.84′N | | 100 m upstream from MA-5, east facing bend | dunite without plagioclase | | | elongated olivine (1:2), oriented; cpx and plagioclase are intercumulate; most of cpx is altered |

**Table 1.** (continued)

| Sample | Massif | Type | Longitude–Latitude | Outcrop | Local Description | Rock Description | Orientation | Outcrop Description | Thin Section Observation |
|---|---|---|---|---|---|---|---|---|---|
| OM95-12 | Ibra/Samail | dunite | 23°6.04′N, 57°58.30′E | (1007 m) | wadi east of tuff (elevation 1007 m) | Dn-Gb contact, contact is slightly faulted | gabbro dike (310°, 50°S) | gabbro sills are approximately horizontal, parallel to Moho observed near the ridge; low-temperature faults cut across all over, above 50 m section; massive dunite continues above a big fault; is this possible displacement? | cpx is interstitial |
| OM95-19 | Ibra/Samail | gabbro | 23°10.15′N, 58°02.44′E | (1231 m) | Wadi Sayjani (1231 m), near the peak (1458 m), on the ridge | gabbro, part of layered section | | this gabbro probably belongs to lower crust section, since we have crossed the Moho | euhedral olivine; anhedral cpx altering to amphibole; large plagioclase |
| OM95-20 | Ibra/Samail | gabbro | 23°11.35′N, 58°0.68′E | (~600 m) | at the marging of two wadi; the small wadi goes to the table top, the other one is Sayjani. | gabbro | | | olivine is altering to amphibole and serpentinite, rim is mostly reacted; opx is abundant; plagioclase is small; hetradocumulate texture |
| OM95-30 | Ibra/Samail | gabbro | approximately 23°09′N, 58°18′E | | entrance of Wadi Sayjani from Ibra Road | gabbro at layered part, next to OM95-31 | | Moho appeared to be cut by a fault; gabbro also appeared to be intruded by peridotite; OM95-31 includes intrusion of metaperidotite | large plagioclase; poikilitic amphibole surround cpx and plagioclase; cpx is euhedral; heteradocumulate texture |
| OM95-32 | Ibra/Samail | gabbro | approximately 23°09′N, 58°18′E | | near Sayjani, by Ibra Road, east side | part of layered gabbro | | faulted contact with peridotite; since contact is faulted, this is less likely Moho | plagioclase abundant with altered rim; cpx is changing to amphibole |

**Table 1.** (continued)

| Sample | Massif | Type | Longitude–Latitude | Outcrop | Local Description | Rock Description | Orientation | Outcrop Description | Thin Section Observation |
|---|---|---|---|---|---|---|---|---|---|
| OM95-49 | Ibra/Samail | wehrlite | 23°3.09′N, 57°55.84′E | (~960 m) | Wadi Sayma branching off from the road heading north | interlayered with gabbro; altered | | wehrlite is interlayered with gabbro, but contact geometry is kinking instead of straight | olivine is elongated, oriented, and serpentinized; plagioclase and cpx are altered to clay mineral; heteradocumulate texture |
| OM95-52 | Ibra/Samail | gabbro | 23°4.75′N, 58°3.10′E | (785 m) | Wadi Suqt | gabbro, thin layered | parallel to Moho | first layered sill intrusion of 8–10 m thick; it seems parallel to Moho | plagioclase is altering to clay; cpx and olivine are altering to amphibole; overall, heteradocumulate texture |
| OM95-53 | Ibra/Samail | gabbro | 23°4.67′N, 58°2.71′E | (~850 m) | Wadi Suqt | gabbro, layered | parallel to Moho | second layered sill | heteradocumulate texture with many triple junctions; cpx and olivine are altering |
| OM95-54 | Ibra/Samail | wehrlite | 23°4.65′N, 58°2.68′E | (~875 m) | Wadi Suqt, 50 m vertical of last GPS fix | dunite | | above the second layer, probably ~10 m thick | cpx is ploikilocrastic and altering to amphibole |
| OM95-56 | Ibra/Samail | olivine gabbro | 23°4.41′N, 58°2.53′E | (~1000 m) | Wadi Suqt | gabbro, layered | parallel to Moho | gabbro sill above dunite with massive fracture and impregnation | plagioclase is large (~2 mm), altering to clay; cpx is interstitial, worm-like-shaped crystals, psuedo-poikiloblastic; olivine is serpentinized |
| OM95-57 | Ibra/Samail | gabbro | 23°4.42′N, 58°2.52′E | (1043 m) | Wadi Suqt, sample is collected at 30 m above | gabbro, layered | parallel to Moho | | plagioclase rims are altering; cpx is subhedral, altering to amphibole |

**Table 1.** (continued)

| Sample | Massif | Type | Longitude–Latitude | Outcrop | Local Description | Rock Description | Orientation | Outcrop Description | Thin Section Observation |
|---|---|---|---|---|---|---|---|---|---|
| OM95-58 | Ibra/Samail | gabbro | 23°8.54′N, 58°8.13′E | | by Ibra Road | | | | cpx is heavily altered; plagioclase shows adcumulus growth; rim is zoned |
| OM97-1 | Wadi Tayin | wehrlite | 22°53.94′N, 58°28.34′E | | Wadi Aqsaybah | | | | poikilitic texture, olivine included in cpx oikocrysts; altered plagioclase is present; textural relationship between plagioclase and olivine is not clear |
| OM97-2 | Wadi Tayin | wehrlite | 22°53.94′N 58°28.34′E | | Wadi Aqsaybah | | | | poikilitic texture, olivine included in cpx oikocrysts; altered plagioclase is present |
| OM98-200 | Wadi Tayin | wehrlite | 23°26.1′N 57°40.1′E | | Wadi Aqsaybah | | | | poikilitic texture, olivine included in cpx oikocrysts; altered plagioclase is present |
| OM98-201 | Wadi Tayin | wehrlite | 22°53.94′N 58°28.34′E | | Wadi Aqsaybah | | | | poikilitic texture, olivine included in cpx oikocrysts; altered plagioclase is present |

**Table 2.** Modal Analysis for Sample[a]

| Sample | Rock Type | *X* | *Y* | Olivine | ± | Enstatite | ± | Spinel | ± | Diopside | ± | Plagioclase | ± | n.d. | Counts |
|---|---|---|---|---|---|---|---|---|---|---|---|---|---|---|---|
| OM94-30 | troctolite (M) | 1 | 1 | 82.8 | 3.4 | | | 2.0 | 0.5 | | | 15.2 | 1.5 | | 711 |
| OM94-31 | wehrlite (plagioclase) | 1 | 1 | 79.7 | 3.6 | 1.1 | 0.4 | 0.8 | 0.4 | 12.8 | 1.4 | 5.5 | 0.9 | | 617 |
| OM94-32A[b] | troctolite 1 | 1 | 1 | 22.8 | 2.3 | 0.2 | 0.2 | | | | | 77.0 | 4.3 | | 421 |
| OM94-32A[b] | anorthosite 1 | 1 | 1 | 1.0 | 0.6 | | | | | 0.3 | 0.3 | 98.7 | 5.6 | | 312 |
| OM94-32A[b] | anorthosite 2 | 0.6 | 0.6 | | | 0.3 | 0.3 | | | 7.1 | 1.5 | 92.6 | 5.2 | | 337 |
| OM94-32A[b] | troctolite 2 | 0.6 | 0.6 | 45.9 | 4.0 | | | 0.4 | 0.4 | | | 53.7 | 4.4 | | 281 |
| OM94-32A[b] | troctolite 3 | 0.6 | 0.6 | 69.2 | 2.9 | | | | | | | 30.8 | 1.9 | | 814 |
| OM94-34 | dunite | 1 | 1 | 95.7 | 3.4 | 0.1 | 0.1 | 2.7 | 0.6 | 1.5 | 0.4 | | | | 820 |
| OM94-35[b] | olivine gabbro (M) | 1 | 1 | 44.4 | 2.2 | 12.9 | 1.2 | | | 7.7 | 0.9 | 29.7 | 1.8 | 5.2 | 935 |
| OM94-36 | wehrlite (plagioclase) | 1.3 | 1.2 | 63.5 | 3.5 | 0.6 | 0.3 | 4.2 | 0.9 | 18.6 | 1.9 | 13.1 | 1.6 | | 521 |
| OM94-37 | dunite | 1.6 | 1.6 | 84.0 | 3.6 | 0.8 | 0.3 | 2.0 | 0.5 | 1.8 | 0.5 | 11.4 | 1.3 | | 656 |
| OM94-38 | dunite | 1.6 | 1.6 | 95.8 | 4.6 | | | 3.1 | 0.8 | | | 1.1 | 0.5 | | 448 |
| OM94-39 | dunite 1 | 1 | 1 | 95.2 | 3.4 | 0.4 | 0.2 | 1.2 | 0.4 | 0.2 | 0.2 | 3.0 | 0.6 | | 831 |
| OM94-39 | dunite 2 | 0.6 | 0.6 | 95.0 | 3.7 | | | 3.1 | 0.7 | 1.4 | 0.4 | 0.4 | 0.2 | | 707 |
| OM95-12 | dunite | 1 | 1 | 92.2 | 9.1 | | | 6.9 | 1.0 | 0.8 | 0.4 | | | | 1066 |
| OM95-19 | olivine gabbro | 0.67 | 0.6 | 6.2 | 1.2 | 4.1 | 1.4 | | | 17.9 | 2.8 | 71.9 | 7.2 | | 913 |
| OM95-20 | olivine gabbro | 0.67 | 0.6 | 7.9 | 1.4 | 11.6 | 1.7 | | | 23.9 | 1.8 | 56.6 | 3.8 | | 828 |
| OM95-30[b] | gabbro | 0.333 | 0.4 | | | 0.1 | 0.2 | | | 47.6 | 4.0 | 52.3 | 3.6 | | 1222 |
| OM95-32[b] | gabbro | 0.67 | 0.6 | | | | | | | 29.1 | 3.1 | 70.9 | 2.9 | | 1423 |
| OM95-49 | wehrlite (plagioclase) | 1 | 1 | 72.4 | 6.3 | | | 3.6 | 0.7 | 7.0 | 1.2 | 17.1 | 2.1 | | 1212 |
| OM95-52[b] | gabbro | 1 | 1 | 0.8 | 0.5 | 6.6 | 1.7 | | | 32.3 | 2.3 | 60.3 | 3.2 | | 1239 |
| OM95-53[b] | olivine gabbro | 0.33 | 0.4 | 5.9 | 1.1 | 8.0 | 2.1 | 0.1 | 0.1 | 29.1 | 2.8 | 57.0 | 3.9 | | 1277 |
| OM95-54 | wehrlite | 1 | 1 | 80.4 | 5.9 | 1.4 | 0.6 | 4.1 | 0.8 | 12.4 | 1.8 | 1.7 | 0.6 | | 1044 |
| OM95-56[b] | olivine gabbro | 0.67 | 0.6 | 19.8 | 1.6 | 1.2 | 0.4 | | | 0.9 | 0.4 | 78.1 | 5.3 | | 1205 |
| OM95-57[b] | olivine gabbro | 1 | 1 | 5.7 | 1.2 | | | | | 32.7 | 2.4 | 61.7 | 4.1 | | 1375 |
| OM95-58 | gabbro | 1 | 1 | | | 2.1 | 1.0 | | | 2.6 | 1.3 | 52.8 | 7.6 | 42.5 | 610 |

[a]Units are in vol %. Errors (±) are determined using the equation proposed by *Solomon* [1963]. Here, "n.d." is a phase that is heavily weathered, and primary phase was not determined. Counts are the total counts performed on the thin section. *X* and *Y* columns are the grid spacing in millimeters. "(M)" denotes olivine-rich samples, while "(plagioclase)" denotes the presence of plagioclase in wehrlite. The following samples are not analyzed for modes: 84OG5B, 90OA65D, 91OA132B, OM97-1, OM97-2, OM98-200, and OM98-201.

[b]Reported by *Kelemen et al.* [1997b].

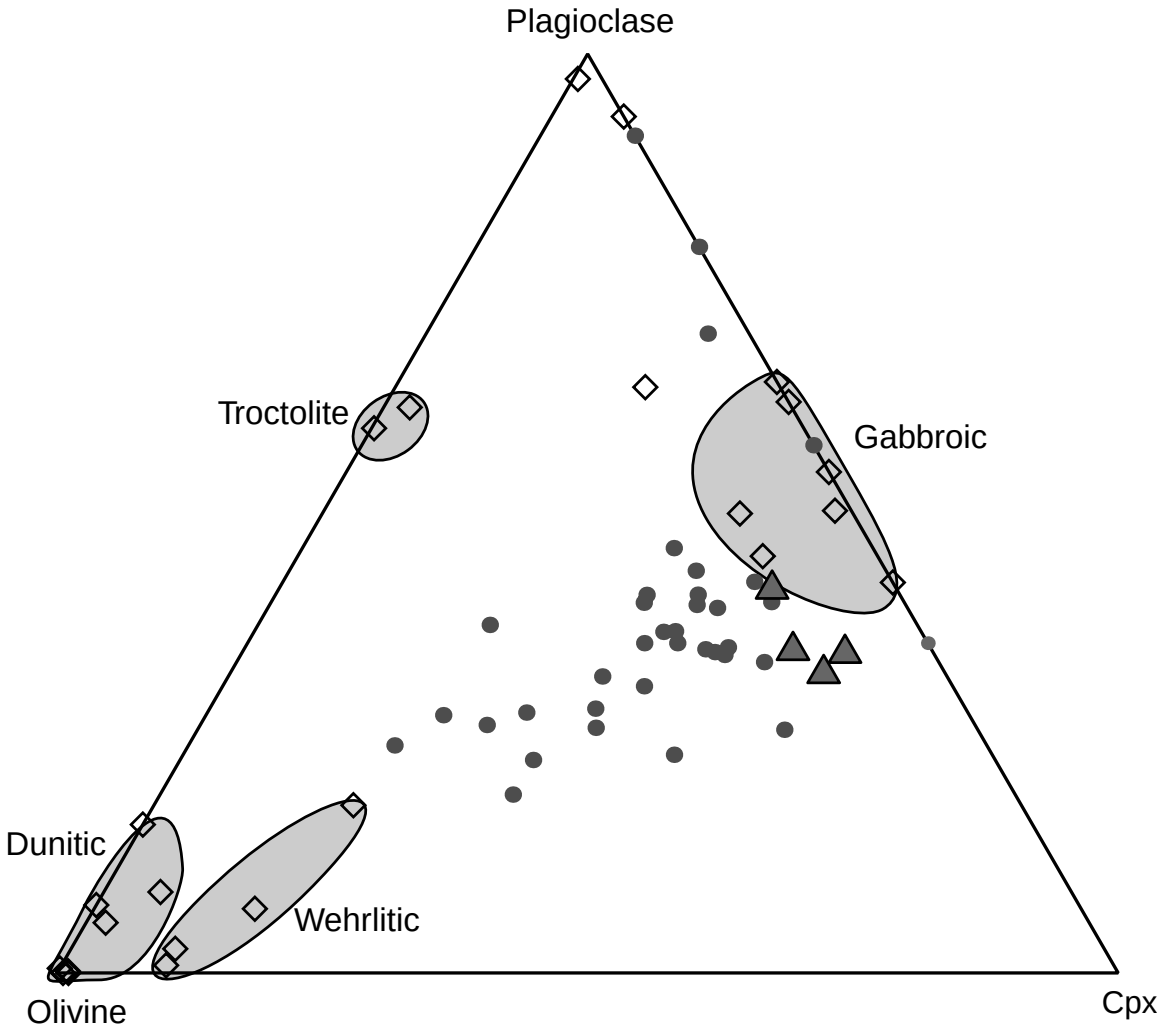


**Figure 3.** Primary modal composition of rock samples based on point counting, indicated with open diamonds, projected on the clinopyroxene-olivine-plagioclase plane. Upward triangles show three phase-saturated liquidus compositions calculated by *Korenaga and Kelemen* [1997] using the crystal fractionation model of *Grove et al.* [1992] for four model magma compositions. The initial primary compositions are from *Kinzler and Grove* [1992a, 1992b, 1993], *Browning* [1982], and *Pallister* [1984]. Gray circles are modal compositions determined for gabbros from the Maqsad area MTZ [*Korenaga and Kelemen*, 1997] and the gabbroic crustal section of the Wadi Tayin massif (P. B. Kelemen and C. J. Garrido, manuscript in preparation, 2001).

for Ti, V, Cr, Zr, Sr, and Y. We used a 20 eV energy window and a −60 V energy offset, with a five-cycle, 30 s counting routine for rare earth element (REE) analysis. The primary beam current was adjusted so that the intensity of $^{30}$Si was ∼2000–3000 counts/s. Trace element concentrations were measured only on clinopyroxene crystals. When a sample contained enough clinopyroxene crystals, at least three were analyzed for each sample, and at least two points in one grain in each sample were analyzed. Analytical uncertainty of REE

is 12–15% and ~5–8% for other trace elements, based on the counting statistics and on repeated analyses of clinopyroxene standards.

## 4. Results and Discussion

### 4.1. Modes and Textural Observations

[17] The dunitic rocks are texturally distinct from gabbroic sills. This distinction suggests different deformation histories for the two rock types although they occur together. Olivines in our dunite samples are elongated and show a strong lattice-preferred orientation, inferred from the similar extinction angle of most crystals in cross-polarized light. Olivine in gabbro sills shows various deformation textures from elongated to relatively round olivine crystals. Often, gabbros are layered, with alternating bands of high olivine abundance and high plagioclase abundance [e.g., *Korenaga and Kelemen*, 1997]. The bands vary in thickness, but they are generally on the order of 1–10 cm thick.

[18] Most wehrlitic rocks are heavily serpentinized. Olivine elongation is not evident, but relict olivine crystals show a common extinction angle under cross-polarized light, suggesting the existence of a lattice-preferred orientation. Unaltered portions of the samples show a poikilitic texture, with clinopyroxene including small olivines. Locally, olivine crystals are also surrounded by alteration phases replacing plagioclase, interpreted as a relict poikilitic texture. We note that the relative sequence of clinopyroxene and plagioclase crystallization cannot be inferred from the plagioclase-bearing samples. Instead, the similarity of texture and field occurrence between wehrlitic samples from the Maqsad area in the Samail massif and "true" wehrlite found at Wadi Aqsaybah in the Wadi Tayin massif [*Pallister and Hopson*, 1981] is the evidence used to infer the crystallization sequence olivine-clinopyroxene-plagioclase for the wehrlitic rocks.

[19] Projection of modal compositions (Table 2) onto the olivine-plagioclase-diopside plane allows distinction between the different lithologies (Figure 3). Gabbroic rocks from the Oman MTZ analyzed in this study (open diamonds in a gray field) define a broad region close to the normative composition of basalts saturated in olivine, plagioclase, and clinopyroxene at low pressure (triangles). Gabbroic lenses from the Maqsad MTZ [*Korenaga and Kelemen*, 1997] and the crustal section of the Wadi Tayin massif (P. B. Kelemen and C. J. Garrido, manuscript in preparation, 2001) (shown as circles) extend toward more olivine-rich compositions. Two troctolites from our study (parts of gabbroic lenses) have cotectic proportions of olivine and plagioclase, suggesting that they formed as "cumulates" during fractional crystallization. In contrast, wehrlitic rocks do not show cotectic proportions of olivine and clinopyroxene (approximately 70% clinopyroxene) and, instead, are very olivine rich.

### 4.2. Major Element Mineral Compositions

[20] Tables 3–7 report the major element compositions of clinopyroxene, olivine, plagioclase, spinel, and orthopyroxene, respectively. Reported uncertainties are 1 standard deviation from the average for each mineral phase in a rock sample. While compositional variation within or among olivine crystals is limited, other minerals show measurable compositional variation as reported in Tables 3–7.

[21] The fraction of molar anorthite in plagioclase (An) ranges from 0.80 to 0.95 in our samples. The highest values of An in our samples are, unlike plagioclase compositions,

**Table 3.** Average Compositions of Clinopyroxene[a]

| Sample | Rock | $N$[b] | $SiO_2$ | ±[c] | $TiO_2$ | ± | $Al_2O_3$ | ± | $Cr_2O_3$ | ± | FeO | ± | MgO | ± | CaO | ± | MnO | ± | $Na_2O$ | ± | Total | Mg #[d] | $X$(Ca)[e] |
|---|---|---|---|---|---|---|---|---|---|---|---|---|---|---|---|---|---|---|---|---|---|---|---|
| OM94-34 | dunite | 8 | 52.12 | 0.49 | 0.30 | 0.04 | 3.97 | 0.43 | 1.33 | 0.36 | 2.13 | 0.19 | 16.13 | 0.29 | 24.88 | 0.62 | 0.05 | 0.03 | 0.65 | 0.22 | 101.9 | 0.93 | 0.48 |
| OM94-37 | dunite | 2 core | 54.51 | 0.13 | 0.15 | 0.06 | 1.31 | 0.00 | 0.14 | 0.06 | 2.29 | 0.08 | 17.82 | 0.12 | 25.23 | 0.19 | 0.04 | 0.03 | 0.20 | 0.03 | 101.7 | 0.93 | 0.48 |
| OM94-37 | dunite | 1 | 51.35 | 0.63 | 0.72 | 0.03 | 4.27 | 0.18 | 1.31 | 0.05 | 3.14 | 0.04 | 15.92 | 0.36 | 24.21 | 0.46 | 0.09 | 0.00 | 0.40 | 0.03 | 101.4 | 0.90 | 0.47 |
| OM94-39 | dunite | 5 | 53.21 | 0.64 | 0.24 | 0.07 | 2.94 | 0.59 | 1.24 | 0.24 | 2.10 | 0.20 | 16.75 | 0.66 | 23.74 | 1.42 | 0.06 | 0.05 | 0.48 | 0.03 | 100.8 | 0.93 | 0.47 |
| OM95-12 | dunite | 3 | 55.03 | 0.46 | 0.05 | 0.03 | 0.47 | 0.53 | 0.03 | 0.05 | 1.41 | 0.30 | 17.51 | 0.45 | 25.57 | 0.07 | 0.02 | 0.02 | 0.02 | 0.01 | 100.1 | 0.96 | 0.50 |
| OM95-12 | dunite | 4 | 52.19 | 1.12 | 0.14 | 0.11 | 3.28 | 0.87 | 0.03 | 0.01 | 3.70 | 0.73 | 15.75 | 0.62 | 25.67 | 0.17 | 0.02 | 0.03 | 0.01 | 0.01 | 100.8 | 0.88 | 0.49 |
| OM95-12 | dunite | 1 | 52.73 | | 0.00 | | 2.55 | | 0.02 | | 2.57 | | 16.70 | | 25.28 | | 0.01 | | 0.16 | | 100.0 | 0.92 | 0.49 |
| 91OA132B | gabbro | 17 | 52.86 | 0.59 | 0.27 | 0.04 | 3.39 | 0.58 | 0.90 | 0.07 | 3.28 | 0.42 | 17.47 | 0.65 | 23.26 | 1.24 | 0.13 | 0.03 | 0.34 | 0.08 | 101.3 | 0.90 | 0.44 |
| 91OA132B | gabbro | 9 | 51.57 | 0.79 | 0.26 | 0.03 | 4.15 | 0.57 | 0.90 | 0.03 | 3.32 | 0.39 | 17.11 | 0.54 | 23.14 | 1.01 | 0.12 | 0.04 | 0.28 | 0.05 | 101.1 | 0.90 | 0.44 |
| 91OA132B | gabbro | 3 | 52.29 | 0.17 | 0.24 | 0.05 | 3.58 | 0.02 | 0.82 | 0.04 | 3.47 | 0.30 | 17.68 | 0.66 | 23.06 | 0.95 | 0.13 | 0.00 | 0.30 | 0.04 | 101.8 | 0.90 | 0.44 |
| 91OA132B | gabbro | 29 | 52.24 | 0.79 | 0.26 | 0.05 | 3.71 | 0.58 | 0.88 | 0.07 | 3.35 | 0.42 | 17.42 | 0.66 | 23.15 | 1.24 | 0.13 | 0.04 | 0.31 | 0.08 | 101.4 | 0.90 | 0.44 |
| OM94-32A | gabbro | 6 | 52.99 | 0.42 | 0.51 | 0.04 | 2.26 | 0.38 | 0.45 | 0.04 | 3.52 | 0.09 | 16.83 | 0.28 | 23.56 | 0.29 | 0.09 | 0.05 | | | 100.2 | 0.89 | 0.46 |
| OM94-32A | gabbro | 8 | 52.99 | 0.28 | 0.42 | 0.04 | 2.16 | 0.24 | 0.63 | 0.12 | 2.88 | 0.20 | 17.39 | 0.33 | 23.63 | 0.49 | 0.08 | 0.05 | | | 100.2 | 0.91 | 0.46 |
| OM94-35 | gabbro | 10 | 52.34 | 0.58 | 0.25 | 0.03 | 3.27 | 0.41 | 0.96 | 0.15 | 3.34 | 0.24 | 16.97 | 0.44 | 23.10 | 0.65 | 0.09 | 0.04 | | | 100.3 | 0.90 | 0.45 |
| OM94-35 | gabbro | 1 | 50.97 | | 0.24 | | 4.10 | | 0.95 | | 3.92 | | 16.06 | | 22.75 | | 0.07 | | | | 99.1 | 0.88 | 0.45 |
| OM95-30 | gabbro | 8 core | 52.86 | 0.28 | 0.41 | 0.02 | 2.20 | 0.07 | 0.10 | 0.02 | 6.19 | 0.14 | 15.76 | 0.21 | 22.39 | 0.12 | 0.15 | 0.04 | 0.36 | 0.03 | 100.4 | 0.82 | 0.44 |
| OM95-30 | gabbro | 5 rim | 53.47 | 0.50 | 0.33 | 0.04 | 1.96 | 0.09 | 0.10 | 0.04 | 5.82 | 0.14 | 15.48 | 0.06 | 22.75 | 0.09 | 0.14 | 0.01 | 0.31 | 0.02 | 100.4 | 0.83 | 0.45 |
| OM95-52 | gabbro | 13 | 52.46 | 0.21 | 0.32 | 0.02 | 2.85 | 0.20 | 0.25 | 0.02 | 4.83 | 0.08 | 16.69 | 0.29 | 22.46 | 0.14 | 0.10 | 0.03 | 0.18 | 0.02 | 100.1 | 0.86 | 0.44 |
| OM95-58 | gabbro | 6 core | 52.93 | 0.28 | 0.25 | 0.04 | 1.23 | 0.14 | 0.13 | 0.03 | 8.24 | 0.18 | 14.75 | 0.17 | 21.97 | 0.26 | 0.26 | 0.02 | 0.27 | 0.03 | 100.0 | 0.76 | 0.44 |
| OM95-58 | gabbro | 6 rim | 52.82 | 0.09 | 0.23 | 0.04 | 1.24 | 0.13 | 0.11 | 0.02 | 8.50 | 0.08 | 14.28 | 0.05 | 21.91 | 0.16 | 0.28 | 0.06 | 0.28 | 0.01 | 99.6 | 0.75 | 0.44 |
| OM95-19 | olivine gabbro[b] | 9 core | 52.43 | 0.36 | 0.40 | 0.03 | 2.48 | 0.23 | 0.40 | 0.04 | 5.43 | 0.21 | 16.27 | 0.36 | 22.69 | 0.50 | 0.15 | 0.02 | | | 100.3 | 0.84 | 0.44 |
| OM95-19 | olivine gabbro | 9 rim | 52.65 | 0.44 | 0.37 | 0.04 | 2.17 | 0.26 | 0.38 | 0.04 | 5.19 | 0.18 | 16.39 | 0.24 | 22.97 | 0.33 | 0.12 | 0.03 | | | 100.3 | 0.85 | 0.45 |
| OM95-20 | olivine gabbro[b] | 18 | 52.21 | 0.63 | 0.33 | 0.11 | 1.52 | 0.46 | 0.18 | 0.07 | 7.88 | 0.43 | 14.98 | 0.25 | 22.67 | 0.67 | 0.23 | 0.03 | | | 100.0 | 0.77 | 0.45 |
| OM95-53 | olivine gabbro[b] | 13 | 51.96 | 0.26 | 0.46 | 0.03 | 3.16 | 0.21 | 0.25 | 0.04 | 5.99 | 0.11 | 16.11 | 0.19 | 21.69 | 0.09 | 0.14 | 0.02 | 0.27 | 0.02 | 100.0 | 0.83 | 0.42 |
| OM95-56 | olivine gabbro[b] | 8 core | 52.54 | 0.44 | 0.55 | 0.06 | 2.84 | 0.38 | 0.95 | 0.16 | 3.50 | 0.15 | 17.10 | 0.35 | 22.58 | 0.40 | 0.10 | 0.04 | 0.27 | 0.02 | 100.4 | 0.90 | 0.44 |
| OM95-56 | olivine gabbro[b] | 5 rim | 52.85 | 0.26 | 0.54 | 0.02 | 2.55 | 0.31 | 0.89 | 0.10 | 3.16 | 0.16 | 17.49 | 0.30 | 22.34 | 0.79 | 0.09 | 0.02 | 0.25 | 0.04 | 100.2 | 0.91 | 0.44 |
| OM95-57 | olivine gabbro[b] | 8 core | 52.38 | 0.23 | 0.26 | 0.13 | 3.42 | 0.22 | 0.72 | 0.33 | 3.50 | 0.10 | 17.10 | 0.45 | 22.37 | 0.09 | 0.09 | 0.02 | 0.30 | 0.05 | 100.2 | 0.90 | 0.44 |
| OM95-57 | olivine gabbro[b] | 9 rim | 51.96 | 0.29 | 0.51 | 0.12 | 3.30 | 0.30 | 1.12 | 0.14 | 3.82 | 0.10 | 16.53 | 0.26 | 22.23 | 0.10 | 0.11 | 0.03 | 0.36 | 0.02 | 99.9 | 0.89 | 0.44 |
| 84OG5B | troctolite | 5 | 53.09 | 1.12 | 0.36 | 0.01 | 2.39 | 0.60 | 0.00 | 0.00 | 2.55 | 0.23 | 18.11 | 0.61 | 23.44 | 1.01 | 0.00 | 0.00 | 0.11 | 0.07 | 100.0 | 0.93 | 0.45 |
| 84OG5B | troctolite | 6 | 53.60 | 0.72 | 0.32 | 0.06 | 2.09 | 0.79 | 0.00 | 0.00 | 2.40 | 0.39 | 18.18 | 0.53 | 24.39 | 1.21 | 0.00 | 0.00 | 0.09 | 0.05 | 101.1 | 0.93 | 0.46 |
| 84OG5B | troctolite | 11 | 53.35 | 1.12 | 0.34 | 0.06 | 2.24 | 0.79 | 0.00 | 0.00 | 2.47 | 0.39 | 18.14 | 0.61 | 23.91 | 1.21 | 0.00 | 0.00 | 0.10 | 0.07 | 100.6 | 0.93 | 0.45 |

**Table 3.** (continued)

| Sample | Rock | $N$[b] | $SiO_2$ | ±[c] | $TiO_2$ | ± | $Al_2O_3$ | ± | $Cr_2O_3$ | ± | FeO | ± | MgO | ± | CaO | ± | MnO | ± | $Na_2O$ | ± | Total | Mg #[d] | $X$(Ca)[e] |
|---|---|---|---|---|---|---|---|---|---|---|---|---|---|---|---|---|---|---|---|---|---|---|---|
| OM95-32 | troctolite | 8 core | 52.16 | 0.37 | 0.50 | 0.07 | 2.65 | 0.20 | 0.30 | 0.09 | 6.31 | 0.19 | 15.52 | 0.28 | 22.22 | 0.20 | 0.17 | 0.03 | 0.44 | 0.04 | 100.3 | 0.81 | 0.44 |
| OM95-32 | troctolite | 5 rim | 52.41 | 0.16 | 0.40 | 0.03 | 2.42 | 0.11 | 0.26 | 0.04 | 5.98 | 0.11 | 15.87 | 0.21 | 22.54 | 0.23 | 0.15 | 0.01 | 0.39 | 0.02 | 100.4 | 0.83 | 0.44 |
| 90OA65D | wehrlite | 9 | 51.11 | 0.16 | 0.33 | 0.08 | 4.01 | 0.28 | 1.05 | 0.07 | 5.80 | 0.38 | 16.17 | 0.58 | 22.12 | 1.20 | 0.15 | 0.05 | 0.30 | 0.04 | 101.4 | 0.83 | 0.42 |
| 90OA65D | wehrlite | 1 | 51.82 | | 0.25 | | 3.56 | | 0.92 | | 3.20 | | 16.85 | | 23.99 | | 0.12 | | 0.39 | | 100.9 | 0.90 | 0.46 |
| OM94-31 | wehrlite | 16 | 52.08 | 0.54 | 0.28 | 0.03 | 3.27 | 0.34 | 1.31 | 0.17 | 3.01 | 0.28 | 17.01 | 0.57 | 22.96 | 0.72 | 0.09 | 0.03 | | | 100.0 | 0.91 | 0.45 |
| OM94-36 | wehrlite | 6 core | 51.93 | 0.32 | 0.22 | 0.03 | 3.52 | 0.36 | 1.27 | 0.03 | 3.21 | 0.21 | 16.82 | 0.68 | 22.84 | 0.80 | 0.04 | 0.03 | | | 99.9 | 0.90 | 0.45 |
| OM94-36 | wehrlite | 7 rim | 51.81 | 0.62 | 0.21 | 0.02 | 3.40 | 0.46 | 1.27 | 0.09 | 2.85 | 0.17 | 16.71 | 0.44 | 23.75 | 0.33 | 0.09 | 0.04 | | | 100.1 | 0.91 | 0.46 |
| OM95-54 | wehrlite | 9 | 54.22 | 1.09 | 0.23 | 0.25 | 1.19 | 1.02 | 0.32 | 0.14 | 2.41 | 0.69 | 16.81 | 0.88 | 25.18 | 0.10 | 0.12 | 0.04 | 0.10 | 0.01 | 100.6 | 0.93 | 0.49 |
| OM95-54 | wehrlite | 5 | 51.85 | 0.24 | 0.47 | 0.05 | 3.40 | 0.27 | 1.52 | 0.12 | 3.32 | 0.22 | 16.86 | 0.45 | 22.05 | 0.05 | 0.09 | 0.03 | 0.37 | 0.02 | 99.9 | 0.90 | 0.44 |
| OM95-49 | wherlite | 8 | 51.98 | 0.25 | 0.37 | 0.01 | 3.84 | 0.08 | 1.27 | 0.04 | 4.18 | 0.09 | 16.44 | 0.22 | 22.28 | 0.12 | 0.05 | 0.04 | 0.31 | 0.02 | 100.7 | 0.88 | 0.44 |
| OM95-49 | wherlite | 5 | 51.94 | 0.10 | 0.37 | 0.02 | 3.52 | 0.24 | 1.10 | 0.13 | 3.47 | 0.11 | 15.80 | 0.17 | 23.51 | 0.47 | 0.10 | 0.03 | 0.40 | 0.03 | 100.2 | 0.89 | 0.47 |

[a]Values are in wt %. OM97-1, OM97-2, OM98-200, and OM98-201 are not analyzed for major element compositions.

[b]Values indicate number of analyses. More than one average for a rock illustrates heterogeneous mineral compositions: "Core" and "rim" are averages of zoned crystals, and when this is not noted, ranges of compositions are found in different regions of a thin section.

[c]Values are 1 standard deviation of average.

[d]Mg # = molar Mg/(Mg + Fe).

[e]$X$(Ca) = molar Ca/(Mg + Fe + Ca).

**Table 4.** Average Compositions of Olivine

| Sample | Rock | *N* | $SiO_2$ | ± | $TiO_2$ | ± | $Al_2O_3$ | ± | $Cr_2O_3$ | ± | FeO | ± | MgO | ± | CaO | ± | MnO | ± | NiO | ± | Total | Mg # |
|---|---|---|---|---|---|---|---|---|---|---|---|---|---|---|---|---|---|---|---|---|---|---|
| OM94-34 | dunite | 3 | 41.08 | 0.18 | 0.03 | 0.02 | 0.04 | 0.02 | 0.03 | 0.00 | 49.51 | 0.69 | 9.76 | 0.21 | 0.25 | 0.01 | 0.17 | 0.01 | 0.24 | 0.03 | 101.1 | 0.90 |
| OM94-37 | dunite | 3 | 40.64 | 0.25 | 0.02 | 0.03 | 0.04 | 0.02 | 0.02 | 0.03 | 46.44 | 0.06 | 11.13 | 0.17 | 0.03 | 0.04 | 0.11 | 0.05 | 0.16 | 0.02 | 98.6 | 0.88 |
| OM94-39 | dunite | 4 | 41.06 | 0.13 | 0.05 | 0.04 | 0.04 | 0.03 | 0.01 | 0.02 | 50.35 | 0.18 | 8.70 | 0.08 | 0.06 | 0.01 | 0.14 | 0.04 | 0.20 | 0.04 | 100.6 | 0.91 |
| OM95-12 | dunite | 10 | 40.39 | 0.38 | 0.01 | 0.01 | 0.08 | 0.10 | 0.06 | 0.02 | 49.60 | 0.61 | 10.84 | 0.17 | 0.10 | 0.02 | 0.14 | 0.04 | 0.21 | 0.04 | 101.4 | 0.89 |
| 91OA132B | gabbro | 3 | 39.82 | 0.26 | 0.02 | 0.01 | 0.07 | 0.02 | 0.06 | 0.02 | 47.86 | 0.33 | 12.03 | 0.09 | 0.06 | 0.01 | 0.14 | 0.07 | 0.17 | 0.03 | 100.2 | 0.88 |
| OM95-52 | gabbro | 4 | 39.02 | 0.16 | 0.00 | 0.00 | 0.06 | 0.01 | 0.06 | 0.03 | 44.80 | 0.41 | 16.70 | 0.44 | 0.03 | 0.03 | 0.29 | 0.05 | 0.12 | 0.03 | 101.1 | 0.83 |
| OM94-35 | olivine gabbro | 5 | 40.25 | 0.22 | 0.07 | 0.02 | 0.06 | 0.02 | 0.10 | 0.03 | 46.59 | 0.45 | 12.13 | 0.02 | 0.04 | 0.01 | 0.15 | 0.25 | 0.21 | 0.02 | 59.9 | 0.87 |
| OM95-19 | olivine gabbro | 6 | 38.63 | 0.12 | 0.09 | 0.02 | 0.07 | 0.02 | 0.09 | 0.05 | 41.36 | 0.35 | 20.93 | 0.02 | 0.07 | 0.04 | 0.24 | 0.21 | 0.15 | 0.02 | 63.4 | 0.78 |
| OM95-53 | olivine gabbro | 11 | 39.02 | 0.35 | 0.06 | 0.02 | 0.03 | 0.02 | 0.10 | 0.03 | 42.11 | 0.26 | 19.60 | 0.21 | 0.09 | 0.04 | 0.25 | 0.04 | 0.09 | 0.04 | 101.4 | 0.79 |
| OM95-56 | olivine gabbro | 10 | 40.17 | 0.28 | 0.01 | 0.01 | 0.05 | 0.02 | 0.06 | 0.02 | 48.58 | 0.71 | 11.59 | 0.31 | 0.06 | 0.02 | 0.14 | 0.05 | 0.25 | 0.04 | 100.9 | 0.88 |
| OM95-57 | olivine gabbro | 7 | 39.96 | 0.06 | 0.06 | 0.01 | 0.02 | 0.02 | 0.07 | 0.02 | 45.72 | 0.20 | 12.90 | 0.21 | 0.08 | 0.02 | 0.16 | 0.04 | 0.21 | 0.03 | 99.2 | 0.86 |
| 84OG5B | troctolite | 3 | 40.33 | 0.22 | 0.03 | 0.06 | 0.06 | 0.01 | 0.06 | 0.03 | 48.97 | 0.06 | 9.77 | 0.06 | 0.05 | 0.01 | 0.15 | 0.01 | 0.29 | 0.04 | 99.7 | 0.90 |
| OM94-32A | troctolite | 4 | 41.05 | 0.64 | 0.07 | 0.03 | 0.08 | 0.01 | 0.06 | 0.03 | 49.06 | 0.34 | 11.07 | 0.02 | 0.03 | 0.01 | 0.11 | 0.14 | 0.16 | 0.05 | 60.9 | 0.89 |
| 90OA65D | wehrlite | 2 | 38.58 | 0.00 | 0.00 | 0.00 | 0.04 | 0.01 | 0.06 | 0.03 | 41.68 | 0.37 | 18.23 | 0.38 | 0.12 | 0.00 | 0.28 | 0.00 | 0.20 | 0.02 | 99.2 | 0.80 |
| 90OA65D | wehrlite | 1 incl.[a] | 38.36 | | 0.06 | | 0.02 | | 0.13 | | 42.17 | | 18.55 | | 0.05 | | 0.30 | | 0.21 | | 99.8 | 0.80 |
| OM94-31 | wehrlite | 6 | 40.40 | 0.14 | 0.06 | 0.02 | 0.05 | 0.02 | 0.06 | 0.02 | 48.16 | 0.44 | 10.88 | 0.01 | 0.04 | 0.01 | 0.15 | 0.15 | 0.24 | 0.02 | 60.1 | 0.89 |
| OM94-36 | wehrlite | 6 | 40.42 | 0.34 | 0.06 | 0.01 | 0.07 | 0.01 | 0.07 | 0.04 | 48.85 | 0.44 | 11.16 | 0.01 | 0.05 | 0.02 | 0.13 | 0.09 | 0.19 | 0.07 | 60.9 | 0.89 |
| OM95-49 | wehrlite | 9 | 39.82 | 0.52 | 0.00 | 0.00 | 0.08 | 0.07 | 0.07 | 0.02 | 46.88 | 0.91 | 13.41 | 0.22 | 0.12 | 0.06 | 0.18 | 0.05 | 0.22 | 0.03 | 100.8 | 0.86 |
| OM95-54 | wehrlite | 9 | 40.38 | 0.14 | 0.05 | 0.02 | 0.03 | 0.02 | 0.08 | 0.03 | 48.84 | 0.21 | 10.70 | 0.16 | 0.08 | 0.04 | 0.14 | 0.03 | 0.33 | 0.02 | 100.6 | 0.89 |

[a]Here, "1 incl." denotes olivine recognized as chadacryst.

**Table 5.** Average Compositions of Plagioclase

| Sample | Rock | *N* | $SiO_2$ | ± | $Al_2O_3$ | ± | FeO | ± | MgO | ± | CaO | ± | $K_2O$ | ± | $Na_2O$ | ± | Total | *X*(An)[a] | ± |
|---|---|---|---|---|---|---|---|---|---|---|---|---|---|---|---|---|---|---|---|
| OM94-37 | dunite | 1 rim | 47.06 | | 33.09 | | 0.29 | | 0.20 | | 17.65 | | 0.00 | | 1.79 | | 100.08 | 0.85 | |
| OM94-37 | dunite | 3 | 47.47 | 0.11 | 34.56 | 0.09 | 0.12 | 0.04 | 0.01 | 0.01 | 17.53 | 0.51 | 0.02 | 0.02 | 1.80 | 0.02 | 101.52 | 0.84 | 0.01 |
| 91OA132B | gabbro | 2 | 45.85 | 0.18 | 34.74 | 0.29 | 0.14 | 0.00 | 0.01 | 0.00 | 18.36 | 0.18 | 0.01 | 0.01 | 1.19 | 0.01 | 100.30 | 0.89 | 0.02 |
| OM95-30 | gabbro | 12 | 48.57 | 0.68 | 33.24 | 0.26 | 0.33 | 0.05 | 0.02 | 0.01 | 16.40 | 0.37 | 0.00 | 0.00 | 2.30 | 0.10 | 100.86 | 0.80 | 0.01 |
| OM95-32 | gabbro | 1 rim | 53.03 | | 30.27 | | 0.13 | | 0.03 | | 12.73 | | 0.00 | | 5.49 | | 101.68 | 0.56 | |
| OM95-32 | gabbro | 12 | 48.56 | 0.34 | 33.25 | 0.29 | 0.33 | 0.04 | 0.03 | 0.01 | 16.46 | 0.25 | 0.00 | 0.01 | 2.23 | 0.15 | 100.86 | 0.80 | 0.01 |
| OM95-52 | gabbro | 1 rim | 45.46 | | 34.23 | | 1.23 | | 0.85 | | 17.86 | | 0.00 | | 1.01 | | 100.63 | 0.91 | |
| OM95-52 | gabbro | 9 | 45.54 | 0.15 | 34.56 | 0.36 | 0.45 | 0.05 | 0.05 | 0.01 | 18.71 | 0.24 | 0.00 | 0.01 | 1.03 | 0.05 | 100.33 | 0.91 | 0.00 |
| OM95-58 | gabbro | 57 | 46.41 | 0.44 | 34.30 | 0.31 | 0.50 | 0.10 | 0.00 | 0.01 | 17.66 | 0.32 | 0.02 | 0.02 | 1.39 | 0.18 | 100.27 | 0.87 | 0.01 |
| OM95-53 | olivine gabbro | 11 | 46.33 | 0.27 | 33.95 | 0.22 | 0.62 | 0.04 | 0.04 | 0.03 | 17.63 | 0.15 | 0.00 | 0.00 | 1.48 | 0.10 | 100.04 | 0.87 | 0.01 |
| OM95-53 | olivine gabbro | 1 rim | 46.34 | | 34.21 | | 0.56 | | 0.04 | | 17.77 | | 0.03 | | 1.28 | | 100.23 | 0.88 | |
| OM95-53 | olivine gabbro | 1 rim | 45.57 | | 34.46 | | 0.46 | | 0.00 | | 17.93 | | 0.00 | | 1.16 | | 99.57 | 0.90 | |
| OM95-56 | olivine gabbro | 12 | 46.95 | 0.21 | 34.13 | 0.10 | 0.35 | 0.07 | 0.06 | 0.02 | 17.74 | 0.11 | 0.00 | 0.01 | 1.49 | 0.04 | 100.72 | 0.87 | 0.00 |
| OM95-57 | olivine gabbro | 5 | 46.40 | 0.64 | 34.11 | 0.08 | 0.41 | 0.02 | 0.01 | 0.01 | 17.67 | 0.25 | 0.01 | 0.01 | 1.40 | 0.16 | 100.01 | 0.87 | 0.01 |
| 84OG5B | troctolite | 1 rim | 44.85 | | 35.11 | | 0.13 | | 0.00 | | 19.53 | | 0.00 | | 0.66 | | 100.39 | 0.94 | |
| 84OG5B | troctolite | 1 rim | 39.55 | | 31.03 | | 2.83 | | 0.11 | | 24.75 | | 0.01 | | 0.03 | | 98.30 | 1.00 | |
| 84OG5B | troctolite | 8 | 45.00 | 0.27 | 35.19 | 0.26 | 0.17 | 0.06 | 0.04 | 0.02 | 19.62 | 0.11 | 0.01 | 0.01 | 0.64 | 0.07 | 100.67 | 0.94 | 0.02 |
| 90OA65D | wehrlite | 3 | 47.22 | 0.14 | 33.88 | 0.13 | 0.37 | 0.06 | 0.07 | 0.02 | 17.83 | 0.03 | 0.02 | 0.02 | 1.70 | 0.16 | 101.09 | 0.85 | 0.01 |

[a]Molar anorthite content *X*(An) = molar Ca/(Ca + Na + K).

**Table 6.** Average Compositions of Spinel

| Sample | Rock | *N* | $SiO_2$ | ± | $TiO_2$ | ± | $Al_2O_3$ | ± | $Cr_2O_3$ | ± | $Fe_2O_3$ | ± | FeO |
|---|---|---|---|---|---|---|---|---|---|---|---|---|---|
| OM94-34 | dunite | 4 | 0.00 | 0.00 | 0.32 | 0.08 | 26.36 | 1.08 | 37.71 | 1.50 | 6.81 | 0.32 | 13.48 |
| OM94-37 | dunite | 2 | 0.00 | 0.00 | 1.10 | 0.02 | 19.82 | 0.63 | 41.11 | 0.04 | 8.20 | 0.33 | 18.81 |
| OM94-39 | dunite | 3 | 0.04 | 0.02 | 0.47 | 0.04 | 21.22 | 0.48 | 42.64 | 1.26 | 6.83 | 0.63 | 17.00 |
| OM95-12 | dunite | 1 core | 0.00 | | 0.00 | | 45.30 | | 20.93 | | 4.64 | | 14.97 |
| OM95-12 | dunite | 2 | 0.07 | 0.02 | 0.18 | 0.02 | 21.37 | 2.04 | 33.66 | 0.21 | 15.99 | 2.00 | 21.39 |
| OM95-12 | dunite | 6 | 0.05 | 0.03 | 0.18 | 0.04 | 26.65 | 1.32 | 32.28 | 2.47 | 11.75 | 2.56 | 19.75 |
| OM94-32A | gabbro | 2 | 0.00 | 0.00 | 0.28 | 0.02 | 27.38 | 2.04 | 34.98 | 2.06 | 6.36 | 0.33 | 20.62 |
| OM94-32A | gabbro | 2 | 0.90 | 1.28 | 0.27 | 0.02 | 32.37 | 2.02 | 31.39 | 1.73 | 3.12 | 3.60 | 21.53 |
| OM94-35 | olivine gabbro | 1 core | 0.00 | | 0.29 | | 38.37 | | 26.67 | | 4.90 | | 16.97 |
| OM94-35 | olivine gabbro | 2 | 0.00 | | 0.36 | | 30.30 | | 33.15 | | 5.54 | | 20.62 |
| OM95-56 | olivine gabbro | 2 | 0.09 | 0.00 | 1.70 | 0.08 | 19.25 | 0.36 | 39.24 | 0.41 | 8.10 | 0.44 | 23.79 |
| 84OG5B | troctolite | 6 | 0.00 | 0.00 | 0.63 | 0.03 | 22.71 | 1.29 | 41.00 | 1.02 | 6.11 | 0.47 | 19.47 |
| 90OA65D | wehrlite | 5 | 0.01 | 0.03 | 1.15 | 0.08 | 20.43 | 0.31 | 30.63 | 0.59 | 16.67 | 0.47 | 26.07 |
| OM94-31 | wehrlite | 5 | 0.00 | 0.00 | 0.49 | 0.14 | 26.36 | 2.36 | 37.98 | 2.23 | 5.72 | 1.10 | 18.35 |
| OM94-31 | wehrlite | 1 rim | 0.00 | | 0.53 | | 26.39 | | 39.08 | | 3.99 | | 20.66 |
| OM95-49 | wehrlite | 6 | 0.04 | 0.02 | 0.60 | 0.15 | 26.74 | 0.89 | 34.99 | 0.80 | 7.30 | 0.63 | 22.30 |
| OM95-54 | wehrlite | 7 | 0.00 | 0.00 | 1.11 | 0.09 | 18.88 | 0.68 | 41.09 | 0.89 | 8.60 | 0.71 | 22.29 |

[a]Cr # = molar Cr/(Cr + Al).

experimentally crystallized from primitive MORB at shallow depth (less than 2 kbar [*Grove et al.*, 1992]). The difficulty of reconciling experimental data with the observation of high-An crystals in MORB and in ophiolites is a well-known problem. High-An plagioclase crystals are known in MORB pillow lava [*Neilsen et al.*, 1993] and in gabbros formed in oceanic lower crust and upper mantle [e.g., *Dick and Natland*, 1996]. Since the cores of zoned plagioclase commonly contain the highest An, and the zoning is thought to be a result of igneous crystal fractionation, high-An plagioclase is probably formed via magmatic processes. Furthermore, diffusivity of NaSi-CaAl exchange in plagioclase at low temperature, with or without water, is slow [*Grove et al.*, 1984; *Liu and Yund*, 1992]. Diffusive re-equilibration does not produce high An, nor is high An a result of low-temperature alteration.

[22] Trace element data presented in section 4.3 show that samples with high-An plagioclase do not have unusually depleted rare earth element patterns. Although ultradepleted melt (UDM) with highly depleted rare earth element patterns has been reported from oceanic spreading ridges [*Sobolev*, 1996; *Sobolev and Shimizu*, 1993] and is inferred to have been a minor component of magmatism in the Oman ophiolite (*Kelemen et al.* [1997a]; *Benoit et al.* [1999], and this paper), such an occurrence remains rare. In contrast, high-An plagioclase is common in our samples and at ridges worldwide. Therefore, although the origin of high-An plagioclase is puzzling, we infer that the presence of high-An plagioclase in our samples is not related to the late stage, depleted lavas reported from northern Oman [Lasail, or V2, *Alabaster et al.*, 1982; *Ernewein et al.*, 1988] or to the small, ultradepleted dikes found in the mantle section of the Samail and Wadi Tayin massifs [*Benoit et al.*, 1999; *Kelemen et al.*, 1997a].

### 4.3. Trace Elements in Clinopyroxene and in Calculated Melt Compositions

[23] Trace element concentration in clinopyroxene was measured in 27 MTZ samples. Over 100 points were measured in more than 70 grains. Reported trace element abundance in clinopyroxene is the average for each sample (Table 8). When minerals were found to be

**Table 6.** (continued)

| ± | MgO | ± | CaO | ± | MnO | ± | NiO | ± | Total | Mg # | ± | Cr #[a] | ± |
|---|---|---|---|---|---|---|---|---|---|---|---|---|---|
| 0.67 | 14.58 | 0.47 | 0.02 | 0.01 | 0.32 | 0.02 | 0.19 | 0.05 | 103.94 | 0.66 | 0.05 | 0.49 | 0.04 |
| 0.01 | 10.99 | 0.19 | 0.01 | 0.02 | 0.43 | 0.02 | 0.19 | 0.01 | 101.92 | 0.51 | 0.01 | 0.58 | 0.02 |
| 0.83 | 12.13 | 0.49 | 0.04 | 0.00 | 0.31 | 0.02 | 0.10 | 0.07 | 104.55 | 0.56 | 0.05 | 0.57 | 0.03 |
| | 16.11 | | 0.02 | | 0.14 | | 0.02 | | 102.13 | 0.66 | | 0.24 | |
| 0.47 | 9.32 | 0.72 | 0.03 | 0.02 | 0.35 | 0.04 | 0.22 | 0.03 | 108.11 | 0.44 | 0.04 | 0.51 | 0.05 |
| 0.59 | 10.98 | 0.33 | 0.02 | 0.02 | 0.29 | 0.02 | 0.09 | 0.06 | 109.40 | 0.50 | 0.03 | 0.45 | 0.06 |
| 0.59 | 9.99 | 0.11 | 0.08 | 0.01 | 0.46 | 0.02 | 0.17 | 0.09 | 105.50 | 0.46 | 0.02 | 0.46 | 0.06 |
| 3.57 | 10.84 | 0.86 | 0.12 | 0.01 | 0.42 | 0.01 | 0.24 | 0.02 | 114.28 | 0.47 | 0.12 | 0.39 | 0.05 |
| | 13.74 | | 0.27 | | 0.24 | | 0.33 | | 101.78 | 0.59 | | 0.32 | |
| | 10.51 | | 0.11 | | 0.39 | | 0.25 | | 101.23 | 0.48 | | 0.42 | |
| 0.47 | 8.15 | 0.25 | 0.07 | 0.03 | 0.50 | 0.02 | 0.10 | 0.02 | 103.04 | 0.38 | 0.02 | 0.58 | 0.02 |
| 0.37 | 10.63 | 0.24 | 0.09 | 0.02 | 0.41 | 0.03 | 0.29 | 0.02 | 104.81 | 0.49 | 0.02 | 0.55 | 0.04 |
| 0.26 | 6.43 | 0.23 | 0.10 | 0.06 | 0.45 | 0.12 | 0.34 | 0.07 | 104.43 | 0.31 | 0.01 | 0.50 | 0.02 |
| 1.07 | 11.68 | 0.62 | 0.09 | 0.03 | 0.41 | 0.05 | 0.24 | 0.02 | 108.89 | 0.53 | 0.06 | 0.49 | 0.07 |
| | 10.27 | | 0.08 | | 0.46 | | 0.27 | | 101.73 | 0.47 | | 0.50 | |
| 0.46 | 9.57 | 0.36 | 0.03 | 0.02 | 0.35 | 0.06 | 0.07 | 0.09 | 105.38 | 0.43 | 0.03 | 0.47 | 0.03 |
| 1.24 | 8.55 | 0.79 | 0.09 | 0.01 | 0.52 | 0.02 | 0.34 | 0.03 | 105.90 | 0.41 | 0.06 | 0.59 | 0.03 |

zoned, rim and core compositions are reported separately. All trace element abundances are normalized to the values for CI chondrite (denoted CN hereinafter) estimated by *Anders and Grevesse* [1989].

[24] Clinopyroxene is the major repository for many incompatible trace elements in gabbroic and ultramafic rocks. As a result, concentrations of some trace elements in clinopyroxene can be used to estimate the composition of melts that could have equilibrated with our samples. This is true for rare earth element abundance, since subsolidus redistribution of rare earth elements among olivine, clinopyroxene, and plagioclase would have a negligible effect on their concentrations in clinopyroxene. In addition, rare earth element diffusivity is very small in clinopyroxene at subsolidus temperatures [*Van Orman et al.*, 1998].

[25] Using experimentally determined clinopyroxene/melt partition coefficients [e.g., *Hart and Dunn*, 1993], we calculated the trace element composition of melts that could have equilibrated with clinopyroxene in our samples. The variation of trace element concentrations, which vary by a factor of ~10 in our samples, can reflect crystal fractionation and/or the presence of compositionally distinct parental melts. However, the ratios of incompatible elements are relatively insensitive to fractionation of olivine, plagioclase, and clinopyroxene over the compositional range bounded by our samples [e.g., *Kelemen et al.*, 1997b, Figures 5c and 5d]. For example, La/Sm cannot change by a factor of 5 via fractionation of olivine gabbro until the initial liquid is 97% crystallized (olivine:plagioclase:clinopyroxene, 5:42:53 by weight, giving bulk partition coefficients of 0.058 and 0.171 for La and Sm, respectively). Given the high magnesium number of minerals in our samples, it is certain that the liquids which crystallized these minerals did not undergo 97% crystallization. Thus substantial variation of incompatible trace element ratios in clinopyroxene can be used to constrain the extent of variation of parental melt compositions in the Oman MTZ.

[26] Both clinopyroxene and calculated liquid rare earth element (REE) compositions are shown in Figures 4, 5, and 6. Figure 4 illustrates REE patterns for the majority of samples.

**Table 7.** Average Compositions of Orthopyroxene

| Sample | Rock | *N* | $SiO_2$ | ± | $TiO_2$ | ± | $Al_2O_3$ | ± | $Cr_2O_3$ | ± | FeO | ± | MgO | ± | CaO | ± | MnO | ± | Total | Mg # | *X*(Ca) |
|---|---|---|---|---|---|---|---|---|---|---|---|---|---|---|---|---|---|---|---|---|---|
| OM95-20 | olivine gabbro | 6 | 53.26 | 0.18 | 0.19 | 0.04 | 0.99 | 0.10 | 0.11 | 0.03 | 20.06 | 0.13 | 24.89 | 0.27 | 0.87 | 0.09 | 0.51 | 0.04 | 100.88 | 0.69 | 0.02 |
| OM95-20 | olivine gabbro | 3 core | 52.90 | 0.24 | 0.19 | 0.02 | 0.92 | 0.06 | 0.12 | 0.01 | 20.98 | 0.34 | 24.40 | 0.21 | 0.86 | 0.09 | 0.57 | 0.04 | 100.95 | 0.67 | 0.02 |
| OM95-19 | olivine gabbro | 4 | 55.10 | 0.22 | 0.14 | 0.02 | 1.16 | 0.04 | 0.23 | 0.03 | 13.41 | 0.14 | 30.18 | 0.20 | 0.79 | 0.07 | 0.30 | 0.02 | 101.31 | 0.80 | 0.01 |
| OM95-19 | olivine gabbro | 4 | 55.06 | 0.50 | 0.13 | 0.03 | 1.22 | 0.04 | 0.23 | 0.05 | 14.02 | 0.13 | 29.12 | 0.54 | 1.05 | 0.21 | 0.31 | 0.02 | 101.14 | 0.79 | 0.02 |

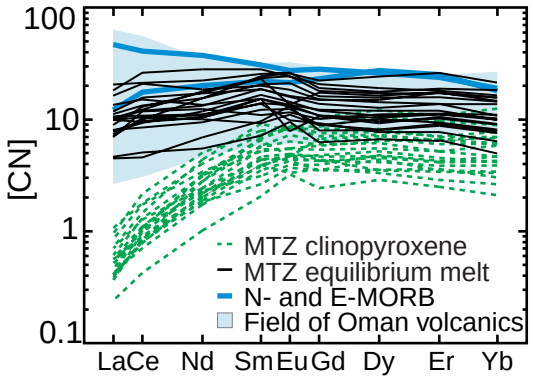


**Figure 4.** REE concentrations in clinopyroxene and calculated melts for 25 of the 27 Oman samples that we analyzed, normalized to the composition of CN [*Anders and Grevesse*, 1989]. REE concentrations in clinopyroxene, measured by ion microprobe, are shown as dashed green lines. Calculated liquid compositions in equilibrium with clinopyroxene are plotted as thin black lines. Averaged normal and enriched MORB compositions from the East Pacific Rise (available from the Geochemical Earth Reference Model (GERM) Web page at http://www.earthref.org/GERM/data /sup2.htm#MORB) are plotted with thick blue lines as a reference. The light blue region shows the range of REE abundances in Oman volcanics and sheeted dikes [*Pallister and Knight*, 1981; *Alabaster et al.*, 1982; *Ernewein et al.*, 1988]. All calculated liquid compositions for these 25 samples have compositions within the range observed in Oman volcanics and show REE concentrations and slopes similar to those of MORB.

Figure 5 shows unusual, relatively light-REE-enriched patterns observed in dunite sample OM94-34. Figure 6 highlights the strongly light-REE-depleted pattern observed in gabbroic sample 84OG5B. Significant depletion of Eu relative to neighboring Sm and Gd (referred to as a "negative Eu anomaly") is absent in most samples, indicating that clinopyroxene precipitated from a melt that had undergone less than 50% crystallization of plagioclase with the high Eu/Sm observed in Oman gabbro plagioclase [*Kelemen et al.*, 1997b, Figures 5c and 5d]. The negative Eu anomaly in a few samples could be due to relatively large degrees of crystal fractionation or to the presence of small proportions of "trapped melt."

#### 4.3.1. A majority of samples recording equilibrium with MORB-like liquids

[27] The majority of the calculated melt REE slopes and concentrations (25 of 27 samples, including ones from the Wadi Tayin area) are similar to those in volcanics and sheeted dikes from the Oman ophiolite (Figure 4). This suggests that the majority of rocks in the MTZ of the Maqsad area were once in equilibrium with melts similar to those which formed the upper crust of the ophiolite. Figure 4 also shows that calculated melts have REE patterns similar to those in "normal" MORB. Since MORB is a mixture of polybaric partial melts of suboceanic mantle, our data suggest that mixing of polybaric melts occurred at or below the MTZ during melt extraction and igneous accretion of the Samail massif in the Oman ophiolite. The nearly

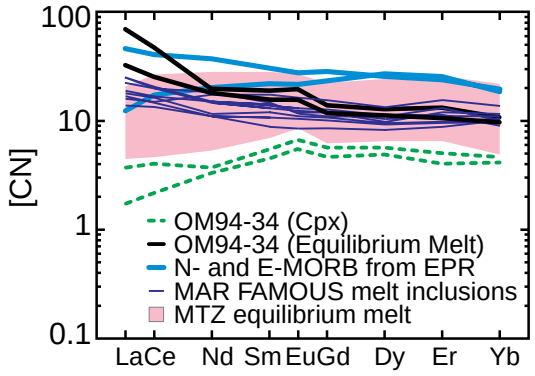


**Figure 5.** Relatively light-REE-enriched, chondrite-normalized patterns of clinopyroxene and calculated liquid in sample OM94-34, shown as dashed green and thick black lines. REE abundances in equilibrium liquid calculated for 25 of our 27 MTZ samples (see Figure 4) are shown with the pink region. MORB compositions are shown by thick blue lines. The composition of some light-REE-enriched melt inclusions from the French-American Mid-Ocean Undersea Study (FAMOUS) region of the Mid-Atlantic Ridge [*Shimizu*, 1998] is shown by thin blue lines.

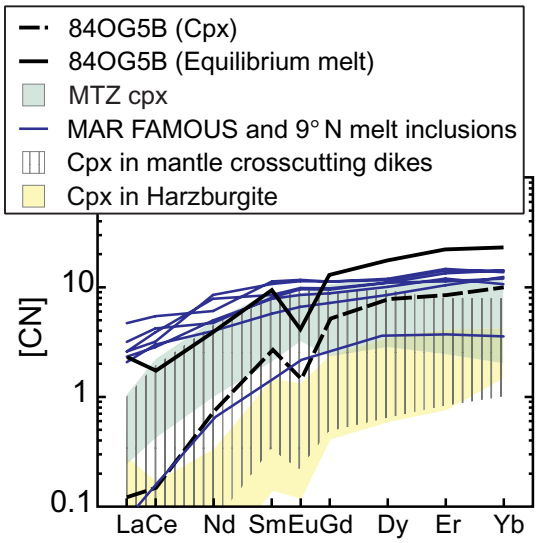


**Figure 6.** Relatively light-REE-depleted patterns of one clinopyroxene and the corresponding calculated liquid in sample 84OG5B normalized to CN, shown as thick black, dashed and solid lines. REE abundance of depleted melt inclusions from the FAMOUS and 9°N regions of the Mid-Atlantic Ridge are shown by thin blue lines [*Sobolev and Shimizu*, 1993; *Shimizu*, 1998]. The melt inclusion with an extremely light-REE-depleted pattern is from the Mid-Atlantic Ridge at 9°N. REE abundance of clinopyroxene in 25 of our 27 MTZ samples (see Figure 4) is shown with the green region. Clinopyroxene REE abundance observed in Oman mantle harzburgite section [*Kelemen et al.*, 1995] is shown as a yellow region. The hatched region shows the composition of websterite and gabbronorite dikes that crosscut the Oman mantle section [*Kelemen et al.*, 1997a].

constant slopes of the REE patterns in clinopyroxenes in our samples are illustrated in a plot of Nd/Yb versus Yb (Figure 7). With the exception of one light-REE-depleted sample, Nd/Yb remains nearly constant over a wide range of Yb concentrations, with a restricted range of variation equivalent to that in glasses from lavas sampled along the East Pacific Rise. Incomplete mixing of high- and low-degree melts from different depths within the melting column beneath an oceanic spreading ridge would produce a correlation between Nd/Yb and Yb. Thus the lack of correlation in Figure 7 suggests that the observed variability in Yb concentration is not primarily due to incomplete mixing of melts derived from different depths and instead is dominated by the effects of crystal fractionation. However, Yb concentration could also have been affected by reaction between early formed crystals and late, interstitial melts.

[28] In passing, we note that MORB-like REE patterns are observed in calculated liquids in equilibrium with clinopyroxene in wehrlite and impregnated dunite as well as gabbroic bodies. Thus we find no support for the idea that magmas parental to wehrlite were more "depleted" than those which formed the gabbroic bodies. We will return to this point in more detail in section 5.2.2.

#### 4.3.2. Sample in equilibrium with light-REE-enriched liquid

[29] Calculated melt in equilibrium with clinopyroxene in sample OM94-34 has a light-REE-enriched pattern (Figure 5). A similar pattern also has been found in melt inclusions in MORB [*Shimizu*, 1998; *Sobolev*, 1996]. Such a melt composition is also inferred from clinopyroxene in some discordant dunites within the mantle section of the Wadi Tayin massif of the Oman ophiolite [*Kelemen et al.*, 1995]. *Sobolev* [1996] attributes such melt compositions to mixtures of polybaric melts that include a relatively high proportion of deep melts derived from small degrees of melting. Alternatively, *Kelemen et al.* [1997a, Figure 1] showed that such light-REE-enriched melts can be produced by shallow reaction between primitive MORB and depleted, residual peridotites.

#### 4.3.3. Sample in equilibrium with light-REE-depleted liquid

[30] Clinopyroxene in sample 84OG5B has a light-REE-depleted pattern (Table 8 and Figure

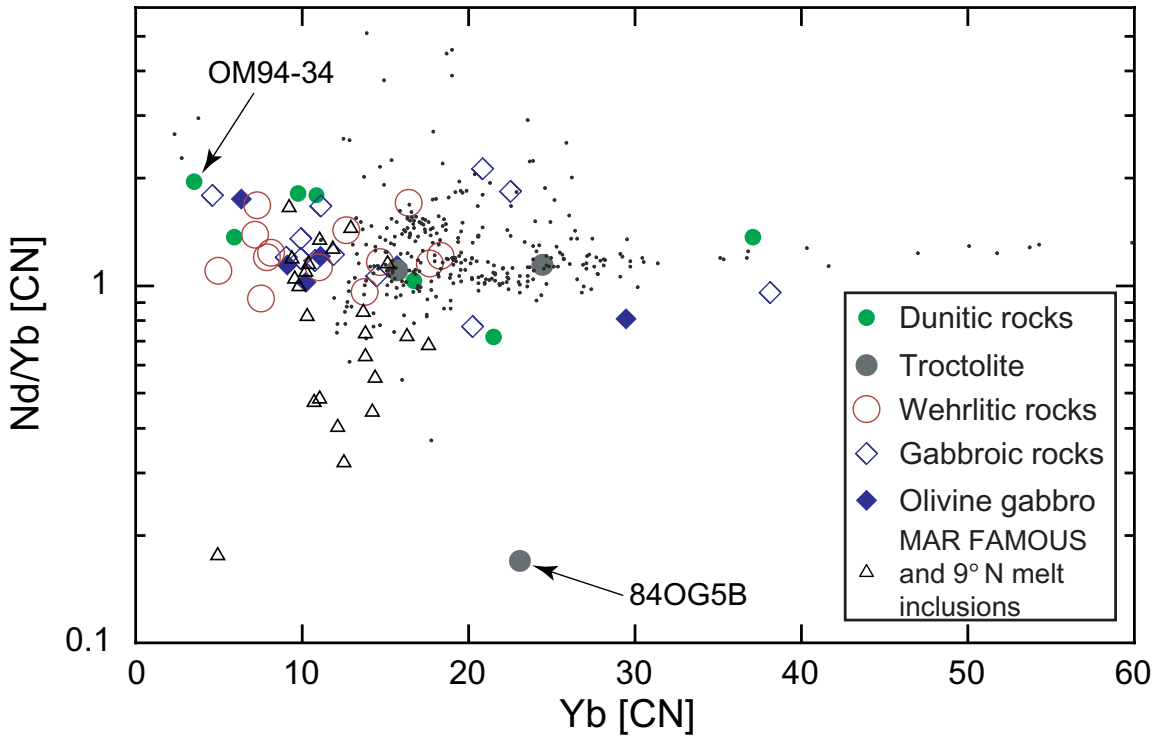


**Figure 7.** Chondrite-normalized Nd/Yb ratios of calculated melt in equilibrium with clinopyroxene in our MTZ samples, shown with circles and diamonds. These ratios show relatively little variation except for the depleted clinopyroxene in sample 84OG5B. Symbols for calculated liquids in equilibrium with clinopyroxene in MTZ samples are as follows: dunitic rocks, solid green circles; troctolites, solid gray circles; wehrlitic rocks, large, red, open circles; gabbroic rocks, large, blue, open diamonds; and olivine gabbros, solid blue diamonds. The small dots are for Nd/Yb in Pacific MORB samples (from the RIDGE Petrological Database, available at http://www.ldeo.columbia.edu/datarep/index.html), for comparison. Small open triangles show Nd/Yb observed in melt inclusions along the Mid-Atlantic Ridge [*Sobolev and Shimizu*, 1993; *Shimizu*, 1998]. Samples with enriched (OM94-34) and depleted (84OG5B) REE patterns are indicated by arrows with sample numbers.

6). Clinopyroxene compositions similar to this are found in narrow gabbronorite and websterite dikes cutting the mantle section of Oman ophiolite [*Benoit et al.*, 1999; *Kelemen et al.*, 1997a, Figure 8]. Such a depleted clinopyroxene REE composition is also found in clinopyroxene in harzburgite in the mantle section of Oman ophiolite [*Kelemen et al.*, 1995] and in clinopyroxene in abyssal peridotite dredged from modern mid-ocean ridges that have been interpreted as residues of mantle melting [*Johnson and Dick*, 1992; *Johnson et al.*, 1990]. These observations suggest that the melt from which troctolite sample 84OG5B crystallized was close to equilibrium with the depleted, shallow mantle section of the Oman ophiolite, which, in turn, was formed as a residue of polybaric, near-fractional melting beneath the Oman spreading ridge.

[31] At modern mid-ocean ridges, depleted melts are observed in olivine-hosted melt inclusions within phenocrysts in lava. For instance, "ultradepleted melts" (UDM) are melts observed in olivine-hosted inclusions reported by *Sobolev and Shimizu* [1993]. The

**Table 8.** Average Trace Element Abundance in Clinopyroxene[a]

| Sample[b] | Type | Points[c] | La | Ce | Sr | Nd | Zr | Sm | Eu | Gd[d] | Ti | Dy | Y | Er | Yb | V | Cr |
|---|---|---|---|---|---|---|---|---|---|---|---|---|---|---|---|---|---|
| OM94-34 | dunite | 4[2c1r.2] | 1.73 | 2.15 | 3.38 | 3.32 | 2.67 | 4.48 | 5.45 | 4.68 | 3.91 | 4.88 | 3.76 | 4.07 | 4.20 | 3.59 | 3.20 |
| OM94-34− | dunite | 1[1r.1] | 3.75 | 4.03 | 3.37 | 3.65 | 2.59 | 5.49 | 6.77 | 5.58 | 3.94 | 5.67 | 4.10 | 5.04 | 4.67 | 3.61 | 3.16 |
| OM94-37 | dunite | 2[2c.2] | 1.64 | 3.39 | 9.05 | 9.52 | 14.26 | 20.86 | 9.97 | 22.89 | 7.06 | 24.92 | 14.78 | 18.07 | 15.94 | 5.37 | 2.30 |
| OM94-37+ | dunite | 1[1c.1] | 0.98 | 1.76 | 0.79 | 3.24 | 0.63 | 4.21 | 6.44 | 4.50 | 1.88 | 4.80 | 7.44 | 7.83 | 7.19 | 2.27 | 0.34 |
| OM94-39 | dunite | 2[1c1r.1] | 0.60 | 1.15 | 0.69 | 2.89 | 1.70 | 7.13 | 8.98 | 8.90 | 4.06 | 10.68 | 6.73 | 10.06 | 9.25 | 3.70 | 2.15 |
| OM95-12 | dunite | 2[2c.2] | 0.78 | 1.20 | 1.28 | 1.29 | 0.26 | 1.60 | 1.40 | 1.67 | 0.40 | 1.73 | 2.53 | 2.13 | 1.51 | 1.94 | 0.05 |
| OM95-21 | dunite | 8[4c4r.3] | 0.50 | 0.65 | 1.28 | 1.51 | 1.09 | 2.70 | 2.14 | 1.95 | 0.35 | 1.20 | 1.29 | 2.07 | 2.54 | 3.62 | 1.71 |
| 91OA132B | gabbro | 5[3c2r.3] | 0.53 | 0.90 | 1.56 | 2.04 | 2.07 | 4.46 | 4.52 | 4.36 | 3.34 | 4.26 | 3.22 | 3.94 | 3.89 | 4.35 | 1.96 |
| 91OA132B− | gabbro | 1[1r.1] | 0.96 | 1.01 | 1.81 | 2.72 | 2.12 | 5.60 | 5.82 | 5.26 | 3.56 | 4.92 | 3.59 | 5.34 | 5.11 | 4.44 | 2.04 |
| 91OA132B− | gabbro | 1[1r.1] | 0.92 | 3.02 | 1.67 | 7.77 | 2.46 | 10.71 | 10.75 | 9.81 | 3.58 | 8.92 | 3.91 | 10.45 | 9.68 | 4.20 | 1.97 |
| OM95-30 | gabbro | 3[3c.3] | 0.72 | 1.30 | 2.38 | 2.53 | 2.04 | 4.45 | 4.74 | 4.87 | 4.68 | 5.29 | 7.39 | 4.66 | 4.27 | 5.25 | 0.19 |
| OM95-32 | gabbro | 2[2c.2] | 0.88 | 1.79 | 1.26 | 3.48 | 3.15 | 5.85 | 6.47 | 6.09 | 5.54 | 6.33 | 9.68 | 5.36 | 4.78 | 5.45 | 0.63 |
| OM95-32+ | gabbro | 1[1c.1] | 0.47 | 0.82 | 1.18 | 1.55 | 2.70 | 2.33 | 2.27 | 2.80 | 4.78 | 3.26 | 8.33 | 1.95 | 1.98 | 4.66 | 0.55 |
| OM95-52 | gabbro | 4[2c2r.3] | 0.42 | 0.80 | 1.72 | 2.22 | 0.99 | 4.81 | 5.02 | 4.79 | 3.68 | 4.77 | 3.96 | 4.31 | 4.27 | 4.16 | 0.45 |
| OM95-52+ | gabbro | 1[1c.1] | 0.95 | 1.08 | 1.90 | 2.37 | 1.19 | 5.32 | 5.72 | 5.65 | 4.39 | 5.98 | 4.55 | 4.20 | 4.63 | 4.57 | 0.57 |
| OM94-35 | olivine gabbro | 5[3c2r.5] | 0.43 | 0.83 | 1.61 | 1.96 | 1.04 | 4.07 | 4.70 | 4.33 | 3.55 | 4.60 | 3.74 | 4.29 | 4.40 | 4.97 | 2.34 |
| OM95-53 | olivine gabbro | 3[2c1r.3] | 0.55 | 1.05 | 2.70 | 3.35 | 1.55 | 6.80 | 8.53 | 7.19 | 6.07 | 7.58 | 5.29 | 6.63 | 6.76 | 5.80 | 0.28 |
| OM95-53+ | olivine gabbro | 1[1c.1] | 0.36 | 0.84 | 1.74 | 2.52 | 1.29 | 4.81 | 5.53 | 5.61 | 5.64 | 6.42 | 4.81 | 5.06 | 4.79 | 6.49 | 0.30 |
| OM95-56 | olivine gabbro | 3[3c.1] | 0.53 | 0.82 | 1.65 | 1.95 | 6.37 | 4.45 | 2.75 | 4.28 | 6.35 | 4.10 | 8.14 | 4.09 | 3.93 | 4.97 | 1.88 |
| OM95-56+ | olivine gabbro | 1[1c.1] | 0.75 | 1.51 | 1.65 | 4.46 | 6.37 | 9.48 | 8.07 | 10.94 | 6.35 | 12.40 | 8.14 | 11.23 | 12.67 | 4.97 | 1.88 |
| OM95-57 | olivine gabbro | 5[3c2r.3] | 0.57 | 0.93 | 1.39 | 2.08 | 0.85 | 4.02 | 3.44 | 3.71 | 2.58 | 3.41 | 3.17 | 2.98 | 2.74 | 3.41 | 2.07 |
| OM95-19− | olivine gabbro | 3[3r.3] | | | 0.93 | | 0.61 | | | | 4.21 | | 5.83 | | | 5.20 | 0.75 |
| OM95-19+ | olivine gabbro | 3[3c.3] | | | 0.98 | | 0.89 | | | | 5.03 | | 6.43 | | | 5.68 | 0.72 |
| OM95-20− | olivine gabbro | 3[3r.3] | | | 0.88 | | 4.02 | | | | 5.21 | | 13.24 | | | 5.72 | 0.20 |
| OM95-20+ | olivine gabbro | 3[3c.3] | | | 0.93 | | 4.87 | | | | 6.04 | | 15.78 | | | 6.00 | 0.29 |
| 84OG5B | troctolite | 3[3c.3] | 0.12 | 0.15 | 0.22 | 0.74 | 1.69 | 2.75 | 1.44 | 5.19 | 3.11 | 7.63 | 6.30 | 8.37 | 9.94 | 5.11 | 2.19 |
| OM94-30 | troctolite | 4[3c1r.2] | 0.82 | 1.71 | 1.19 | 5.26 | 7.69 | 11.00 | 8.96 | 10.39 | 6.43 | 9.79 | 10.93 | 10.34 | 10.51 | 4.82 | 2.33 |
| OM94-32A | troctolite | 6[2c4r.3] | 0.48 | 1.11 | 1.33 | 3.25 | 4.50 | 6.72 | 4.77 | 6.97 | 5.87 | 7.22 | 6.88 | 6.77 | 6.76 | 3.70 | 3.40 |
| 90OA65D | wehrlite | 4[2c2r.2] | 0.24 | 0.39 | 2.04 | 1.30 | 1.48 | 2.82 | 4.62 | 3.19 | 4.44 | 3.56 | 2.72 | 3.40 | 3.24 | 5.57 | 2.33 |

**Table 8.** (continued)

| Sample[b] | Type | Points[c] | La | Ce | Sr | Nd | Zr | Sm | Eu | Gd[d] | Ti | Dy | Y | Er | Yb | V | Cr |
|---|---|---|---|---|---|---|---|---|---|---|---|---|---|---|---|---|---|
| OM97-1− | wehrlite | 3[3r.3] | 0.98 | 2.25 | 1.37 | 5.26 | 3.59 | 8.17 | 8.48 | 8.31 | 4.95 | 8.44 | 7.81 | 7.01 | 7.06 | 4.21 | 2.39 |
| OM97-1+ | wehrlite | 1[1c.1] | 0.42 | 1.13 | 1.52 | 2.29 | 2.83 | 4.26 | 5.00 | 3.95 | 6.69 | 3.64 | 8.17 | 3.71 | 3.13 | 4.65 | 2.40 |
| OM97-2 | wehrlite | 6[4c2r.4] | 0.63 | 1.35 | 1.59 | 3.21 | 2.26 | 5.39 | 5.69 | 6.01 | 5.31 | 6.62 | 7.10 | 6.73 | 6.32 | 4.64 | 3.08 |
| OM98-200 | wehrlite | 3[2c1r.2] | 0.37 | 1.01 | 1.33 | 2.33 | 1.72 | 3.19 | 4.05 | 4.05 | 4.25 | 4.90 | 5.30 | 4.38 | 4.74 | 4.43 | 2.48 |
| OM98-201− | wehrlite | 2[2r.2] | 0.86 | 1.78 | 1.32 | 3.40 | 2.74 | 4.76 | 5.37 | 5.50 | 5.64 | 6.23 | 9.74 | 5.17 | 5.44 | 3.90 | 2.20 |
| OM98-201+ | wehrlite | 2[2c.2] | 0.38 | 0.88 | 1.19 | 1.88 | 1.70 | 2.69 | 3.86 | 3.57 | 4.21 | 4.45 | 5.12 | 3.63 | 3.49 | 3.54 | 2.28 |
| OM94-31 | wehrlite | 4[1c3r.3] | 0.54 | 1.03 | 1.29 | 2.48 | 1.82 | 5.45 | 5.57 | 5.54 | 3.74 | 5.63 | 4.44 | 5.30 | 5.92 | 4.23 | 2.74 |
| OM94-36 | wehrlite | 5[2c3r.3] | 0.43 | 0.73 | 1.85 | 1.78 | 0.94 | 3.55 | 4.34 | 3.58 | 2.83 | 3.61 | 3.09 | 3.52 | 3.39 | 3.75 | 2.69 |
| OM94-36+ | wehrlite | 1[1c.1] | 0.75 | 0.78 | 1.85 | 1.87 | 0.94 | 3.50 | 4.15 | 3.62 | 2.83 | 3.74 | 3.09 | 3.24 | 3.08 | 3.75 | 2.69 |
| OM95-49 | wehrlite | 8[5c3r.5] | 0.25 | 0.44 | 1.93 | 1.03 | 0.89 | 2.08 | 3.32 | 2.51 | 4.58 | 2.94 | 4.36 | 2.56 | 2.14 | 5.96 | 2.43 |
| OM95-54− | wehrlite | 2[2r.2] | 0.98 | 1.80 | 1.03 | 3.84 | 2.59 | 6.65 | 6.23 | 7.06 | 5.14 | 7.47 | 7.63 | 6.11 | 7.60 | 3.98 | 2.74 |
| OM95-54+ | wehrlite | 3[3c.3] | 1.10 | 1.83 | 1.05 | 4.17 | 3.02 | 7.45 | 9.17 | 7.63 | 5.84 | 7.82 | 8.25 | 7.29 | 7.87 | 4.33 | 2.27 |
| CI chondrite, ppm | | | 0.2347 | 0.6032 | 7.8 | 0.4524 | 3.94 | 0.1471 | 0.056 | 0.1966 | 436 | 0.2427 | 1.56 | 0.1589 | 0.1625 | 56.5 | 2660 |
| *D*(cpx/melt) | | | 0.054 | 0.086 | 0.128 | 0.187 | 0.123 | 0.291 | 0.350 | 0.400 | 0.384 | 0.442 | 0.467 | 0.387 | 0.430 | | |

[a]Values are CI chondrite [*Anders and Grevesse*, 1989] normalized using the values shown at the bottom. Partition coefficients, *D*(cpx/melt) for listed elements, are used for calculation of equilibrium melt composition.

[b]Minus and plus signs denote rims and cores of cpx analyses, respectively.

[c]Read 4[2c1r.2] as follows: A total of four points are analyzed, of which four points are core and one is rim of two different crystals.

[d]Gd is calculated by (Eu + Dy)/2.

equilibrium melt composition of 84OG5B, which is shown as a thick solid line in Figure 6, is more enriched in heavy REE than ultradepleted melt inclusions, with heavy REE abundance similar to some depleted lavas from the French-American Mid-Ocean Undersea Study (FAMOUS) area of the Mid-Atlantic Ridge [*Shimizu*, 1998]. However, the ratio of light to middle REE for the equilibrium melt of 84OG5B is very low, closer to ultradepleted melt inclusions than to lavas from FAMOUS (Figures 6 and 7). We conclude that the melt that crystallized 84OG5B was produced by crystal fractionation from a parental liquid similar to ultradepleted melt inclusions. It should be noted that the likelihood of finding UDMs seems to be low, both in the Oman MTZ and in Atlantic melt inclusions. In this study, we have only observed a UDM signature in one sample out of 27, while *Sobolev* [1996] reported one UDM among 120 melt inclusions analyzed.

[32] In the previous paragraph, we have discussed similarities between clinopyroxene in sample 84OG5B and in mantle harzburgite in Oman and from mid-ocean ridges. Also, we have emphasized similarities between the calculated melt composition in equilibrium for sample 84OG5B and melt compositions observed at mid-ocean ridges. However, it is not certain that the melt that crystallized sample 84OG5B had the same origin as those observed along the Mid-Atlantic Ridge. The melt that crystallized sample 84OG5B in the Maqsad MTZ may have been genetically linked to the melts that partially crystallized to form "cumulate" gabbronorite and websterite dikes in the mantle section [*Benoit et al.*, 1999; *Kelemen et al.*, 1997a, Figure 8]. Most of these are undeformed and crosscut the transposed mantle foliation associated with corner flow beneath the Oman spreading ridge. Thus the dikes must have formed at some distance away from the ridge axis, after the shallow

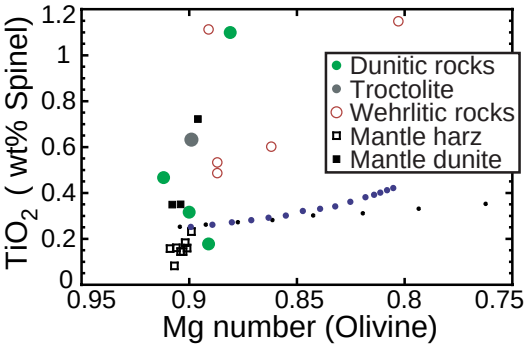


**Figure 8.** $TiO_2$ in spinel versus magnesium number of olivine in our MTZ samples and in mantle samples from the Wadi Tayin massif [*Kelemen et al.*, 1995]. The dotted lines show two models of compositional variation due to crystal fractionation, where each dot corresponds to a 4% increment. The two models use an initial liquid composition of 1.67 wt % $TiO_2$ and a magnesium number of 0.74, which is similar to primitive MORB. The two models are (1) a batch crystallization with 50% clinopyroxene fractionation mode shown by closely spaced larger dots and (2) a fractional crystallization with 95% olivine 5% spinel fractionation mode shown by sparsely spaced smaller dots. The compositional variation in our MTZ dunite samples is not consistent with either origin: via closed system trapped melt shown by batch crystallization model or via open system fractional crystallization. Observed $TiO_2$ concentration is higher than that of the simple fractionation model at a given magnesium number. We used a bulk solid/liquid partition coefficient of (1) 0.197 and (2) 0.011, for $TiO_2$ (assuming fractionation modes with $D$(mineral/liquid) of clinopyroxene [*Hart and Dunn*, 1993], olivine, and spinel [*Kelemen et al.*, 1993]), a bulk solid/liquid partition coefficient of (1) 4.11 and (2) 4.68 for MgO (using the fractionation modes and $D$ predicted at 2 kbar and 1250°C for olivine, clinopyroxene [*Langmuir et al.*, 1992, in Table C1], and spinel), an Fe/Mg $K_D$, where $K_D$ is the exchange reaction constant, between olivine and melt of 0.3, a fractional crystallization expression derived by *Show* [1970] and *Gast* [1968], whose formulae are based on *Rayleigh* [1896], in whose paper $C$(at melt fraction $F$) = $C$(initial) $F^{(D-1)}$, and a batch (equilibrium) crystallization expression in which $C$(at melt fraction $F$) = $C$(initial)/[$D$ − (1 − $F$)$D$].

mantle fabrics were transposed by corner flow [*Kelemen et al.*, 1995, 1997a; *Nicolas et al.*, 2000b]. Furthermore, the dikes have relatively evolved mineral compositions (clinopyroxene magnesium numbers down to 83) compared to residual mantle peridotite, so they must have formed by crystal fractionation from cooling magma within a conductive geotherm, and not within a adiabatic geotherm of the mantle [*Kelemen et al.*, 1997a]. Finally, *Benoit et al.* [1999] have suggested that the melts that formed gabbronorite dikes in the Maqsad mantle section had high $^{87}Sr/^{86}Sr$, indicative of addition of seawater to a mantle source. In the Oman ophiolite this might have occurred during the initiation of obduction, when a thrust fault formed within hot oceanic crust and upper mantle very close to an active spreading ridge [e.g. *Michard et al.*, 1991]. Thus, for a variety of reasons, it is not clear that the melt in equilibrium with our sample 84OG5B formed in the same way as ultra-depleted melt inclusions and depleted lavas found at mid-ocean ridges.

#### 4.3.4. Summary of calculated liquid compositions

[33] In summary, >90% of our samples record equilibration with compositionally indistinguishable parental melts, similar to mid-ocean ridge basalts (MORB) and the melts that formed the crust in Oman. This suggests that mixing of diverse, polybaric partial melts of mantle peridotite occurred at or below the depth of the MTZ. Among 27 samples we found one with light-REE-enriched clinopyroxene and one with light-REE-depleted clinopyroxene. Both have calculated melt compositions that are significantly different from normal MORB lavas. However, such melt compositions are observed in heterogenous, olivine-hosted melt inclusions within MORB. The presence of distinct heterogeneity in <10% of our samples is comparable to the frequency of heterogeneity observed in olivine-hosted melt inclusions in MORB.

## 5. Genesis of Different Lithologies in the MTZ

[34] Observed lithologies in the Maqsad MTZ can be categorized in three groups, as discussed in section 2: dunitic, gabbroic, and wehrlitic rocks. We believe that these rocks were emplaced at the MTZ beneath an active oceanic spreading ridge, since they are high-temperature magmatic rocks and record equilibrium with melts identical to those that formed the overlying gabbros, sheeted dikes, and lavas.

### *5.1. Dunitic Bodies Forming via Melt-Rock Reaction, as Previously Proposed*

[35] In addition to olivine and minor spinel, dunitic rocks (dunite and melatroctolite) commonly include small amounts of interstitial plagioclase and pyroxenes. These are termed "impregnated dunites." Olivine crystals in our dunitic samples are elongated, showing strong deformation, while plagioclase and clinopyroxene are irregularly distributed and do not have a strong crystal shape or lattice fabric. However, plagioclase and clinopyroxene are reported to be "foliated" in other "impregnated dunites" [see also *Boudier and Nicolas*, 1995; *Nicolas and Prinzhofer*, 1983]. Thus it is believed that plagioclase and clinopyroxene crystallized from melt along grain boundary pores in dunites. In some cases, these were affected by subsequent deformation.

[36] The magnesium number of olivine in dunitic rocks is close to the olivine composition in residual peridotites from the Oman mantle section (Table 3 and Figure 8). However, spinel compositions in dunitic rocks from the Maqsad MTZ are distinct from those in the underlying residual mantle harzburgites. Strong

depletion of $TiO_2$ in spinels is observed in mantle residues [*Dick and Natland*, 1996; *Kelemen et al.*, 1995], whereas the MTZ dunitic rocks generally have higher $TiO_2$ in spinel (Figure 8). MTZ dunites have spinel and olivine compositions which overlap those in discordant dunites in the mantle section of the ophiolite, which were interpreted by *Kelemen et al.* [1995] as conduits for focused transport of MORB through the shallow mantle beneath the Oman spreading center. Contact relationships for mantle dunites in Oman and other ophiolites indicate a largely replacive origin, in which olivine-saturated melts ascending via porous flow dissolved pyroxene from residual mantle peridotites (please see *Kelemen et al.* [1995, 1997a, and references therein] for details).

[37] Primitive MORBs also have spinel phenocrysts with high $TiO_2$ [*Kelemen et al.*, 1997a, Figure 5, and references therein]. Thus the relatively high $TiO_2$ in spinels from dunitic rocks in the MTZ and discordant dunites in the mantle section suggests equilibration with MORB-like liquids. Data from our Oman MTZ samples show large variations in spinel $TiO_2$ at nearly constant olivine magnesium number ($TiO_2$ ranges from ~0.1 to 1.1 wt % in spinel, while all but one of our spinel-bearing samples have olivine Mg # between 0.91 and 0.85). In contrast, increasing spinel $TiO_2$ by 0.1 wt % via crystal fractionation should cause olivine Mg # to vary from 0.91 to less than 0.83 (Figure 8). Thus the high spinel $TiO_2$ associated with high olivine Mg # in MTZ and mantle dunite spinels probably arises from equilibration with relatively $TiO_2$-rich primary melts, rather than as a result of crystal fractionation. Indeed, elevation of spinel Ti contents at nearly constant olivine Mg # via reaction between ascending melt and shallow, residual mantle peridotite was proposed by *Dick and Natland* [1996] and *Arai and Matsukage* [1996] for high-Ti spinels in dunites formed along the East Pacific Rise and sampled at Hess Deep. Also, a majority of the clinopyroxene REE patterns and concentrations in our dunitic samples from the MTZ are not distinguishable from those in Oman mantle dunites reported elsewhere [*Kelemen et al.*, 1995, Figure 3].

[38] To summarize, considering (1) the observed variation of Ti and olivine Mg # and (2) the analogy to compositionally identical mantle dunites whose contact relations clearly show that they replaced surrounding peridotite as a result of melt-rock reaction, we confirm the hypothesis based on overall field observations [e.g., *Boudier and Nicolas*, 1995] that most of the dunitic rocks in the MTZ are products of reaction between a MORB-like melt with shallow, residual mantle peridotite.

### 5.2. Impregnated Peridotites: Not Recording Information on Melt Porosity

[39] Some recent studies on impregnated dunites in the Maqsad MTZ, and compositionally and texturally similar impregnated peridotites just below the MTZ, have interpreted the volume and/or shape of interstitial plagioclase and clinopyroxene as a proxy for the volume and/or shape of grain boundary melt pores that were trapped at some time during the formation of the ophiolite [e.g., *Jousselin and Mainprice*, 1998; *Jousselin et al.*, 1998]. However, we believe that these interpretations are incorrect, at least in part.

[40] It is apparent from the major element compositions of the minerals, and from the REE concentrations in clinopyroxene of impregnated dunites and peridotites analyzed for this study (OM94-30, OM94-37, OM94-39, and OM95-12), that interstitial plagioclase and clinopyroxene do not represent trapped melts. As mentioned in section 5.1, the magnesium number of olivine and pyroxene in impregnated dunite and peridotite (0.89–0.91 for olivine and 0.90–0.95

for clinopyroxene) is higher than that for mantle-derived melt beneath an oceanic spreading ridge. The plagioclase An contents in our samples are also higher than the normative An content of mantle-derived melts at spreading ridges. Similarly, the REE concentrations in clinopyroxene of impregnated dunites and peridotites are lower than those of mantle-derived melts at spreading ridges. Thus pyroxene and plagioclase in impregnated dunites and peridotites cannot represent the composition of MORB-like trapped melt.

[41] Furthermore, plagioclase in Oman samples always has a positive Eu anomaly [e.g., *Pallister and Knight*, 1981; *Benoit et al.*, 1996; *Kelemen et al.*, 1997b]. The absence of a corresponding negative Eu anomaly in clinopyroxene (and olivine) in most impregnated dunites and peridotites (in this study, OM94-30, OM94-39, and OM95-12, plus clinopyroxene cores in OM94-37) requires that the whole rocks must have a positive Eu anomaly. Neither residual peridotites nor mantle-derived melts at mid-ocean ridges have a significant, positive Eu anomaly. If the impregated peridotites were mixtures of residual peridotite and trapped melt, the whole rock would have no detectable Eu anomaly. Instead, the presence of a positive Eu anomaly in the whole rock, as for Oman gabbros [*Pallister and Knight*, 1981; *Benoit et al.*, 1996; *Kelemen et al.*, 1997b], indicates the presence of ''cumulate'' plagioclase, which formed during partial crystallization of a melt in an open system from which the remaining melt was removed. *Kelemen et al.* [1997b] showed that for fractional crystallization involving olivine, clinopyroxene, and plagioclase with compositions observed in the Oman MTZ, there would be a detectable Eu anomaly in clinopyroxene after ~50% crystallization. Thus the absence of an Eu anomaly in clinopyroxene in the impregnated peridotites indicates that the melt which crystallized plagioclase and clinopyroxene in these rocks underwent less than ~50% crystallization. Since it has a negative Eu anomaly and high REE contents in clinopyroxene rims, impregnated dunite sample OM94-37 could be an exception to this general observation.

[42] Plagioclase and clinopyroxene in most impregnated peridotites formed by partial crystallization (<50% and, probably, <10%) of a mafic liquid, after which the remaining liquid was removed. This statement, supported by observations discussed in the previous paragraph, adds limitations to interpretations of volume of ''trapped melt'' and ''frozen melt lenses.'' At any given time the pores could have been larger than the observed volume of clinopyroxene + plagioclase in impregnated dunite and peridotite, since the crystals represent a small fraction of the parental liquid mass. Alternatively, the pores could have been smaller than the observed volume of clinopyroxene + plagioclase, since the crystals could have formed over time by gradual accumulation from tiny pores containing migrating liquid. Thus the volume of plagioclase + clinopyroxene places neither an upper nor a lower bound on the instantaneous melt porosity at any time during the genesis of impregnated peridotites.

[43] In some cases, impregnated peridotites preserve a lattice-preferred orientation in olivine, indicative of ductile solid flow, together with undeformed plagioclase + clinopyroxene. In these cases, one can infer that the plagioclase + clinopyroxene crystallized after deformation of the olivine and that the instantaneous melt fraction in the rock during plagioclase + clinopyroxene crystallization did not exceed some critical porosity (many estimates are ~30% [*Renner et al.*, 2000]) at which the solid matrix would disaggregate and the lattice-preferred orientation would be obliterated. However, such an inference does not require any information about the abundance of the plagio-

clase + clinopyroxene impregnations. Again, the abundance of the plagioclase + clinopyroxene impregnations provides no constraint on the instantaneous melt porosity.

[44] It also seems questionable to estimate the shape or topology of a melt phase from the topology of plagioclase + clinopyroxene in impregnated peridotites, even where plagioclase and clinopyroxene are undeformed. The equilibrium texture is determined by the relative surface energies of neighboring phases. In a system undergoing chemical reaction and/or deformation the textural maturity depends on rates of reaction and diffusion [e.g., *Holness and Siklos*, 2000]. A texture recording the topology of melt within a solid matrix could only be preserved in a rock if melt components had insufficient time to diffuse or react to form a texture that is controlled by the surface energy of the crystallizing solid phases. In the limit, such a process would form glass within the rock, as in quenched experiments on melt + dunite or melt + peridotite. Clearly, this limit is not approached in Oman impregnated dunites and peridotites. The chemical components in melt had time to sort themselves out into crystals of olivine + plagioclase + clinopyroxene, and a substantial residual melt fraction had time to escape. In fact, we rarely detect significant zoning in mineral grains within Oman MTZ samples. Thus it seems that diffusion was relatively fast compared to crystallization of clinopyroxene and plagioclase in impregnated peridotites, so that mineral surface energies could have had a large effect on the resulting grain shapes.

[45] To summarize, we conclude that the volume and shape of interstitial plagioclase and clinopyroxene in impregnated dunites and peridotites from the Maqsad MTZ and underlying mantle cannot be used to infer the volume or the shape of melt pores within the rocks at any time during their formation.

#### 5.2.1. Gabbroic bodies: Cumulates from MORB-like liquids, as previously proposed

[46] Our data on MTZ gabbros are consistent with previous work on these rocks. Our samples have clinopyroxene REE patterns consistent with equilibrium with MORB and with the melts that formed the gabbros, sheeted dikes, and lavas of the Oman ophiolite. This observation supports the inference that the gabbroic sills in the MTZ formed beneath an active spreading ridge, rather than at a later time in an off-axis setting [*Kelemen et al.*, 1997b].

[47] Gabbroic sills or lenses in the MTZ include gabbro, troctolite, olivine gabbro, and anorthosite. Our data, combined with previous analyses, show that while the different lithologies probably arise via different degrees of crystal fractionation from a common parental liquid, the differences in extent of crystallization must have been small, judging by the limited range of variability in olivine, clinopyroxene, and plagioclase compositions. Negative Eu anomalies in clinopyroxene are only measurable in three samples (OM94-32A, OM95-56, and OM95-32). Analyzing similar, relatively small Eu anomalies, *Kelemen et al.* [1997b] suggested that gabbroic rocks in the Maqsad MTZ are "cumulates" that represent less than 50% by mass of the parent melt from which they crystallized.

#### 5.2.2. Clinopyroxene in wehrlitic bodies: Indistinguishable from clinopyroxene in gabbroic rocks

[48] Our samples of wehrlitic rocks from the Maqsad MTZ are all plagioclase wehrlites and melagabbros. A true wehrlite was found in Wadi Aqsaybah in the Wadi Tayin massif, where wehrlites had previously been described [*Juteau et al.*, 1988; *Pallister and Hopson*, 1981]. The Wadi Aqsaybah wehrlites intrude lower crustal layered gabbros and show a poikilitic texture, with clinopyroxene oikoc-

rysts including small, rounded olivines [*Pallister and Hopson*, 1981, Figure 3n]. In the Maqsad MTZ, wehrlitic samples also have poikilitic textures, and clinopyroxene and plagioclase are reported as oikocrysts. This texture has been observed in wehrlites intruding crustal gabbros from massifs throughout the Oman ophiolite [*Benn et al.*, 1988; *Juteau et al.*, 1988; *Nicolas et al.*, 1988b; *Reuber*, 1988; *Boudier and Nicolas*, 1995]. Thus it seems, on textural and structural grounds, that all these occurrences of wehrlitic rocks are related.

[49] A variety of workers [*Pallister and Hopson*, 1981; *Benn et al.*, 1988; *Juteau et al.*, 1988; *Nicolas et al.*, 1988b; *Reuber*, 1988; *Boudier and Nicolas*, 1995] have made the following conclusions on the bases of field relationships. Wehrlite intrusions commonly crosscut modal layering in gabbroic host rocks but do not show chilled margins. In many cases, wehrlitic rocks have undergone ductile deformation along with their host gabbros. Thus the wehrlitic intrusions must have occurred while the gabbros were still hot, and therefore near the axis of the Oman spreading center. Also, wehrlites have never been observed intruding the Oman mantle section, so they apparently originate within the MTZ. Olivine in some wehrlitic rocks preserves subgrain boundaries, indicative of plastic deformation, but never or rarely preserves a lattice-preferred orientation.

[50] The presence of true wehrlites demonstrates that some magmas within the Oman MTZ had the crystallization sequence olivine-clinopyroxene-plagioclase and therefore were fundamentally different in some important respect from magmas that crystallized troctolites and gabbro and had the crystallization sequence olivine-plagioclase-clinopyroxene. Until now, one possible interpretation of these data has been that the magmas that formed troctolites were formed by lower degrees of partial melting, and thus had higher Al, Ca, and Na contents, compared to the magmas that formed wehrlites [e.g., *Smewing*, 1981; *Alabaster et al.*, 1982]. This, in turn, suggested that the troctolites, and genetically related gabbroic rocks, were related to the lower Geotimes or V1 lava series whereas the wehrlites might be related to the later, much more depleted, Lasail or V2 lava series which is exposed in the northern massifs of the Oman ophiolite. On the basis of this reasoning we expected the Maqsad and Wadi Aqsaybah wehrlites to record equilibrium with a distinctly REE-depleted melt composition.

[51] MORB-type liquid REE patterns were determined for all wehrlitic rocks, including wehrlite samples from Wadi Aqsaybah (see data for samples OM97-1, OM97-2, OM98-200, and OM98-201). Also, clinopyroxenes in wehrlitic rocks do not have systematically lower trace element concentrations, at a given magnesium number, compared to clinopyroxenes in gabbroic and dunitic rocks from the Maqsad MTZ. Thus the melt that crystallized clinopyroxene in wehrlitic rocks was similar in REE and other trace element contents to the melts that formed clinopyroxene in gabbroic sills and impregnated dunites. As a consequence, it is unlikely that the wehrlites crystallized from a melt that was significantly depleted compared to MORB or the Oman Geotimes/V1 lava series. This supports previous inferences based on the field and textural relationships of wehrlitic rocks [e.g., *Benn et al.*, 1988; *Boudier and Nicolas*, 1995]. We must look for an alternative explanation for the different crystallization sequences in true wehrlites compared to troctolite and gabbroic rocks.

[52] It could be argued that many wehrlitic rocks are simply extreme examples of impregnated peridotites. Where they intrude crustal gabbros, they could represent a crystal-rich mush formed by mobilization of residual man-

tle olivine [e.g., *Benn et al.*, 1988; *Boudier and Nicolas*, 1995]. This hypothesis is supported by a variety of field and petrographic observations, and we see no reason to discard it. However, this hypothesis alone does not explain the difference in crystallization sequence which is implied by the presence of both troctolites (olivine + plagioclase) and true wehrlites (olivine + clinopyroxene) in the Oman MTZ. In this context, also note that plagioclase/clinopyroxene ratios in ''impregnated dunites'' are different from those in wehrlite (Figure 3).

[53] The most likely reason for the difference in crystallization sequence, though it remains speculative, is that aqueous fluids derived from seawater penetrated into magma chambers (probably sills) along the Oman MTZ. This might have occurred via hydrothermal circulation along faults. Addition of $H_2O$ to MORB-like basaltic melts at 2 kbar will suppress the crystallization of plagioclase relative to olivine and clinopyroxene, changing the order of crystallization [e.g., *Gaetani et al.*, 1993]. Because the concentration of most major and trace elements in seawater is much less than the concentration of the same elements in basaltic melt and the amount of aqueous fluid added to magma is limited by the solubility of $H_2O$ at 2 kbar, the addition of seawater-derived aqueous fluid to melt might not have an obvious effect on our geochemical data.

[54] An influx of fluid derived from seawater might be marked by a significant shift in both oxygen and strontium isotope ratios. If our idea is correct, such a shift should be observed in wehrlites, which should have lower $^{18}O/^{16}O$ and higher $^{87}Sr/^{86}Sr$ than spatially related gabbroic rocks. Unfortunately, most or all Oman wehrlites have undergone extensive, low-temperature hydrous alteration, which may alter the isotope signature of earlier, high-temperature interaction between melt and aqueous fluids.

## 6. Conclusions

[55] Three important observations have been made. (1) The majority of our samples of plutonic rocks from the Samail MTZ are close to REE exchange equilibrium with normal MORB. Heterogeneous melts must have formed by polybaric, decompression melting of the mantle beneath the Oman spreading center. Our data imply that most of these different melt compositions were mixed and homogenized at or below the depth of the MTZ. Evidence for the presence of less well mixed melts with variable REE contents was found in <10% of our MTZ samples (2 of 23). (2) Plagioclase and clinopyroxene in impregnated peridotites formed in an open system through which melt was flowing and do not represent the crystalline products of ''trapped melt.'' As a consequence, one cannot infer the proportion or shape of melt-filled pores in these rocks from the volume or shape of plagioclase + clinopyroxene patches. (3) Parental melts that formed wehrlitic rocks had the same REE contents as those which crystallized clinopyroxene, all but two MTZ samples including dunitic rocks, impregnated peridotites, and gabbroic rocks.

[56] In addition, we made some observations that confirm previous hypotheses. (1) Olivine and spinel in MTZ dunites are very similar in composition to olivine and spinel in discordant dunite within the mantle section of the ophiolite, supporting the idea that MTZ dunites form by reaction between MORB-like melt and shallow, residual mantle peridotite. (2) Gabbroic lenses in the MTZ record equilibrium with the melts that formed the overlying gabbros, sheeted dikes, and lavas and therefore probably formed beneath the active Oman spreading ridge, and not later in an off-axis setting.

[57] An overall scenario for the formation of the MTZ can be constrained by our observa-

tions together with previous work. Discordant dunites in the mantle section formed as a result of transport of parental MORB through the uppermost mantle [e.g., *Kelemen et al.*, 1995]. Many, if not all, mantle dunites are products of pyroxene dissolution in olivine-saturated melt moving through the mantle via focused porous flow. Some Maqsad MTZ dunites could be transposed, and later impregnated, relicts of mantle dunites which formed in the upwelling mantle and then underwent corner flow immediately beneath the crust at a spreading center. However, as pointed out by *Jousselin et al.* [1998], formation of additional dunite at the MTZ seems to be required by the presence of a 500 m thick MTZ composed of more than 50% dunite in the Maqsad area. It is unlikely that this thick dunite sequence is composed entirely of transposed, mantle dunite because the largest mantle dunites in Oman are only 100 m thick [*Kelemen et al.*, 2000]

[58] Gabbro sills or lenses formed within dunite in the MTZ. We believe that this was due to pooling of melt beneath a permeability barrier formed by crystallization of melt in pore space at the base of the conductive geotherm extending downward from the seafloor [*Boudier et al.*, 1996; *Kelemen et al.*, 1997b; *Korenaga and Kelemen*, 1997; *Kelemen and Aharonov*, 1998]. At the depth of formation of gabbro sills in the MTZ, melt must have been well mixed to produce nearly identical REE slopes throughout all of our gabbroic samples.

[59] Wehrlitic rocks were the last igneous rock type to form in abundance in the Maqsad MTZ, since they crosscut surrounding gabbroic rocks. However, wehrlitic rocks also record REE exchange equilibrium with MORB-type melts. Also, the lack of chilled margins in wehrlite intrusions, and the fact that some of them underwent high-temperature ductile deformation along with host gabbros, suggest that they formed in a near-ridge environment. The presence of a distinct crystallization sequence in wehrlitic rocks compared to gabbroic rocks and to the normal crystallization sequence of MORB at pressures of 2 kbar or less is tentatively ascribed to the addition of seawater-derived, hydrothermal fluid to magmas within the MTZ.

[60] REE exchange equilibrium with ultradepleted melts was recorded by one MTZ gabbroic sample, as well as by previously reported, small gabbronorite and websterite dikes within the Oman mantle section. These undeformed dikes are filled with "cumulate" minerals which crystallized from cooling magma passing upward through transposed, conductively cooled mantle lithosphere, probably relatively far from an active spreading ridge.

## Acknowledgments

[61] In the course of this research we were supported in part by NSF grants OCE-9819666 (P.B.K.), OCE-9711170 (P.B.K.), and OCE-9416616 (P.B.K., N.S., K.T.K.). We were generously guided in our initial field work in the Oman ophiolite by Adolphe Nicolas, Francoise Boudier, Benoit Ildefonse, and Edwin Gnos, with the support of Hilal Al Azri, Director of the Geological Survey of Oman. We have benefited greatly from many discussions with the mid-ocean ridge and ophiolite research community. Specifically, we would like to thank Joe Cann, Alex Sobolev, and Dan McKenzie for sharing their insights and arguments on the topics of where MORB heterogeneity arises and where mixing occurs. Jun Korenaga shared the result of his crystal fractionation calculations, Henry Dick provided facilities and advice on point counting, Graham Layne and Ken Burrhus provided technical assistance with the ion microprobe, and Nil Chatterjee and Mike Jercenowitz supported our work on the MIT electron microprobe. Using this opportunity, K.T.K. would like to thank Jerry Wasserburg for his words of encouragement during an emotionally difficult time in the field. This manuscript was significantly improved as a result of critical constructive reviews by Adolphe Nicolas, Paul Asimow, Yoshio Tatsumi, and one

anonymous reviewer. Bill White kindly provided editorial support and advice.

## References


Alabaster, T., J. Pearce, and J. Malpas, The volcanic stratigraphy and petrogenesis of the Oman ophiolite complex, *Contrib. Mineral. Petrol.*, *81*, 168–183, 1982.

Albee, L. A., and L. Ray, Correction factors for electron probe microanalysis of silicates, oxides, carbonates, phosphates, and sulfates, *Anal. Chem.*, *42*, 1408–1414, 1970.

Anders, E., and N. Grevesse, Abundances of the elements: Meteoritic and solar, *Geochim. Cosmochim. Acta*, *53*, 197–214, 1989.

Arai, S., and K. Matsukage, Petrology of the gabbro-troctolite-peridotite complex from Hess deep, equatorial Pacific: Implications for mantle-melt interaction within the oceanic lithosphere, *Proc. Ocean Drill. Program Sci. Results*, *147*, 135–155, 1996.

Bence, A. E., and A. L. Albee, Empirical correction factors for the electron microanalysis of silicate and oxides, *J. Geol.*, *76*, 382–403, 1968.

Benn, K., A. Nicolas, and I. Reuber, Mantle-crust transition zone and origin of wehrlite magmas: Evidence from the Oman ophiolite, *Tectonophysics*, *151*, 75–85, 1988.

Benoit, M., M. Polvé, and G. Ceuleneer, Trace element and isotopic characterization of mafic cumulates in a fossil mantle diapir (Oman ophiolite), *Chem. Geol.*, *134*, 199–214, 1996.

Benoit, M., G. Ceuleneer, and M. Polvé, The remelting of hydrothermally altered peridotite at mid-ocean ridges by intruding mantle diapirs, *Nature*, *402*, 514–518, 1999.

Boudier, F., and A. Nicolas, Nature of the Moho transition zone in the Oman ophiolite, *J. Petrol.*, *36*, 777–796, 1995.

Boudier, F., A. Nicolas, and B. Ildefonse, Magma chambers in the Oman ophiolite: Fed from the top and the bottom, *Earth Planet. Sci. Lett.*, *144*, 239–250, 1996.

Browning, P., The petrology, geochemistry, and structure of the plutonic rocks of the Oman ophiolite, Ph.D. thesis, Open Univ., Milton Keynes, England, UK, 1982.

Ceuleneer, G., and M. Rabinowicz, Mantle flow and melt migration beneath oceanic ridge: Models derived from observations in ophiolites, in *Mantle Flow and Melt Generation at Mid-ocean Ridges*, *Geophys. Monogr. Ser.*, vol. 71, edited by J. P. Morgan, D. K. Blackman, and J. M. Sinton, pp. 123–154, AGU, Washington, D. C., 1992.

Ceuleneer, G., A. Nicolas, and F. Boudier, Mantle flow patterns at an oceanic spreading centre: The Oman peridotites record, *Tectonophysics*, *151*, 1–26, 1988.

Coleman, R. G., Tectonic setting for ophiolite obduction in Oman, *J. Geophys. Res.*, *86*, 2497–2508, 1981.

Crawford, W. C., S. C. Webb, and J. A. Hildebrand, Constraints on melt in the lower crustal and Moho at the East Pacific Rise, 9 degrees 48′N, using seafloor compliance measurements, *J. Geophys. Res.*, *104*, 2923–2939, 1999.

Detrick, R. S., P. Buhl, E. Vera, J. Mutter, J. Orcutt, J. Madsen, and T. Brocher, Multi-channel seismic imaging of a crustal magma chamber along the East Pacific Rise, *Nature*, *326*, 35–41, 1987.

Dick, H. J. B., and J. H. Natland, Late-stage melt evolution and transport in the shallow mantle beneath the East Pacific Rise, *Proc. Ocean Drill. Program Sci. Results*, *147*, 103–134, 1996.

Dunn, R. A., and D. R. Toomey, Seismological evidence for three-dimensional melt migration beneath the East Pacific Rise, *Nature*, *388*, 259–262, 1997.

Ernewein, M., C. Pflumio, and H. Whitechurch, The death of an accretion zone as evidenced by the magmatic history of the Sumail ophiolite (Oman), *Tectonophysics*, *151*, 247–274, 1988.

Gaetani, G. A., T. L. Grove, and W. B. Bryan, The influence of the water on the petrogenesis of subduction-related igneous rocks, *Nature*, *365*, 332–334, 1993.

Garmany, J., Accumulations of melt at the base of young oceanic crust, *Nature*, *340*, 628–632, 1989.

Gast, P. W., Trace element fractionation and the origin of tholeiitic and alkaline magma types, *Geochim. Cosmochim. Acta*, *32*, 1057–1086, 1968.

Grove, T. L., M. B. Baker, and R. J. Kinzler, Coupled CaAl-NaSi diffusion in plagioclase feldspar: Experiments and applications to cooling rate speedometry, *Geochim. Cosmochim. Acta*, *48*, 2113–2121, 1984.

Grove, T. L., R. J. Kinzler, and W. B. Bryan, Fractionation of mid-ocean ridge basalt (MORB), in *Mantle Flow and Melt Generation at Mid-ocean Ridges, Geophys. Monogr. Ser.*, vol. 71, edited by J. P. Morgan, D. K. Blackman, and J. M. Sinton, pp. 281–310, AGU, Washington, D. C., 1992.

Hacker, B. R., Rapid emplacement of young oceanic lithosphere: Argon geochronology of the Oman ophiolite, *Science*, *265*, 1563–1565, 1994.

Hart, S. R., and T. Dunn, Experimental cpx/melt partitioning of 24 trace elements, *Contrib. Mineral. Petrol.*, *113*, 1–8, 1993.

Holness, M. B., and S. T. C. Siklos, The rates and extent of textural equilibration in high-temperature fluid-bearing systems, *Chem. Geol.*, *162*, 137–153, 2000.

Johnson, K., and H. Dick, Open system melting and temporal and spatial variation of peridotite and basalt at the Atlantis II fracture zone, *J. Geophys. Res.*, *97*, 9219–9241, 1992.

Johnson, K. M., H. Dick, and N. Shimizu, Melting in the oceanic upper mantle: An ion microprobe study of diopside in abyssal peridotites, *J. Geophys. Res.*, *95*, 2661–2678, 1990.

Jousselin, D., and D. Mainprice, Melt topology and seismic anisotropy in mantle peridotites of the Oman ophiolite, *Earth Planet. Sci. Lett.*, *164*, 553–568, 1998.

Jousselin, D., A. Nicolas, and F. Boudier, Detailed mapping of a mantle diapir below a paleo-spreading center in the Oman ophiolite, *J. Geophys. Res.*, *103*, 18,153–18,170, 1998.

Juteau, T., M. Ernewein, I. Reuber, H. Whitechurch, and R. Dahl, Duality of magmatism in the plutonic sequence of the Sumail nappe, Oman, *Tectonophysics*, *151*, 107–135, 1988.

Kelemen, P. B., and E. Aharonov, Periodic formation of magma fractures and generation of layered gabbros in the lower crust beneath oceanic spreading ridges, in *Faulting and Magmatism at Mid-ocean Ridges*, *Geophys. Monogr. Ser.*, vol. 106, edited by W. R. Buck, et al., pp. 267–289, AGU, Washington, D. C., 1998.

Kelemen, P. B., N. Shimizu, and T. Dunn, Relative depletion of niobium in some arc magmas and the continetal crust: partitioning of K, Nb, La and Ce during melt/rock reaction in the upper mantle, *Earth Planet. Sci. Lett.*, *120*, 111–134, 1993.

Kelemen, P. B., N. Shimizu, and V. J. M. Salters, Extraction of mid-ocean-ridge basalt from the upwelling mantle by focused flow of melt in dunite channels, *Nature*, *375*, 747–753, 1995.

Kelemen, P. B., G. Hirth, N. Shimizu, M. Spiegelman, and H. J. B. Dick, A review of melt migration processes in the adiabatically upwelling mantle beneath oceanic spreading ridges, *Philos. Trans. R. Soc. London, Ser. A*, *355*, 283–318, 1997a.

Kelemen, P. B., K. Koga, and N. Shimizu, Geochemistry of gabbro sills in the crust/mantle transition zone of the Oman ophiolite: Implications for the origin of the oceanic lower crust, *Earth Planet. Sci. Lett.*, *146*, 475–488, 1997b.

Kelemen, P. B., M. Braun, and G. Hirth, Spatial distribution of melt conduits in the mantle beneath oceanic spreading ridges: Observations from the Ingalls and Oman ophiolites, *Geochem Geophys. Geosyst.*, vol. 1, Paper number 1999GC000012 [8266 words, 8 figures, 1 table]. Published July 11, 2000.

Kent, G., A. Harding, and J. Orcutt, Evidence for a smaller magma chamber beneath the East Pacific Rise at 9°30′N, *Nature*, *344*, 650–653, 1990.

Kinzler, R. J., and T. L. Grove, Primary magmas of mid-ocean ridge basalts, 1, Experiments and methods, *J. Geophys. Res.*, *97*, 6885–6906, 1992a.

Kinzler, R. J., and T. L. Grove, Primary magmas of mid-ocean ridge basalts, 2, Applications, *J. Geophys. Res*, *97*, 6907–6926, 1992b.

Kinzler, R. J., and T. L. Grove, Corrections and further discussion of the primary magmas of mid-ocean ridge basalts, 1 and 2, *J. Geophys. Res*, *98*, 22,339–22,347, 1993.

Klein, E. M., and C. H. Langmuir, Global correlations of ocean ridge basalt chemistry with axial depth and crustal thickness, *J. Geophys. Res.*, *92*, 8089–8115, 1987.

Korenaga, J., and P. B. Kelemen, Origin of gabbro sills in the Moho transition zone of the Oman ophiolite: Implications for magma transport in the oceanic lower crust, *J. Geophys. Res.*, *102*, 27,729–27,749, 1997.

Langmuir, C. H., E. M., Klein, and T. Plank, Petrological systematics of mid-ocean ridge basalts: Constraints on melt generation beneath ocean ridges, in *Mantle Flow and Melt Generation at Mid-ocean Ridges, Geophys. Monogr. Ser.*, vol. 71, edited by J. P. Morgan, D. K. Blackman, and J. M. Sinton, pp. 183–280, AGU, Washington, D. C., 1992.

Liu, M., and R. A. Yund, NaSi-CaAl interdiffusion in plagioclase, *Am. Mineral.*, *77*, 275–283, 1992.

Michard, A., F. Boudier, and B. Goffe, Obduction versus subduction and collision in the Oman case and other Tethyan settings, in *Ophiolite Genesis and Evolution of the Oceanic Lithosphere*, edited by T. Peters, A. Nicolas, and R. Coleman, pp. 447–467, Kluwer Acad., Norwell, Mass., 1991.

Neilsen, R. L., R. Bourgeois, K. Haskell, L. Forsythe, D. M. Christie, and M. R. Fisk, Melt inclusions in high-An feldspar from the Gorda Ridge: Examples of melt diversity, *Eos Trans. AGU, 74* (43), Fall Meet. Suppl., F644, 1993.

Nicolas, A., A melt extraction model based on structural studies in mantle peridotites, *J. Petrol.*, *27*, 999–1022, 1986.

Nicolas A., *Structure of Ophiolites and Dynamics of Oceanic Lithosphere*, 367 pp., Kluwer Acad., Norwell, Mass., 1989.

Nicolas, A., and A. Prinzhofer, Cumulative or residual origin for the transition zone in ophiolite: Structural evidence, *J. Petrol.*, *24*, 188–206, 1983.

Nicolas, A., G. Ceuleneer, F. Boudier, and M. Misseri, Structural mapping in the Oman ophiolites: Mantle diapirism along an oceanic ridge, *Tectonophysics*, *151*, 27–56, 1988a.

Nicolas, A., I. Reuber, and K. Benn, A new magma chamber model based on structural studies in the Oman ophiolite, *Tectonophysics*, *151*, 87–105, 1988b.

Nicolas, A., F. Boudier, B. Ildefonse, and E. Ball, Accretion of Oman and United Arab Emirates ophiolite: Discussion of a new structural map, *Mar. Geophys. Res.*, *21*, 147–179, 2000a.

Nicolas, A., B. Ildefonse, F. Boudier, X. Lenoir, and W.B. Ismail, Dike distribution in the Oman-United Arab Emirates ophiolite, *Mar. Geophys. Res.*, *21*, 269–287, 2000b.

Pallister, J. S., Paret magmas of the Samail ophiolite, Oman, in *Ophiolites and Oceanic Lithosphere*, *Geol. Soc. Spec. Publ.*, *13*, *63–70*, 1984.

Pallister, J. S., and C. A. Hopson, Samail ophiolite plutonic suite: Field relations, phase variations, cryptic variation and layering, and a model of a spreading ridge magma chamber, *J. Geophys. Res.*, *86*, 2593–2644, 1981.

Pallister, J. S., and R. J. Knight, Rare-earth element geochemistry of the Samail ophiolite near Ibra, Oman, *J. Geophys. Res.*, *86*, 2673–2697, 1981.

Prinzhofer, A., and C. J. Allegre, Residual peridotites and the mechanisms of partial melting, *Earth Planet. Sci. Lett.*, *74*, 251–265, 1985.

Rayleigh, J. W. S., Theoretical consideration respecting the separation of gases by diffusion and similar processes, *Philos. Mag.*, *42*, 493–498, 1896.

Renner, J., B. Evans, and G. Hirth, On the rheologically critical melt fraction, *Earth Planet. Sci. Lett.*, *181*, 585–594, 2000.

Reuber, I., Complexity of the crustal sequence in the northern Oman ophiolite (Fizh and southern Aswad blocks): The effect of early slicing?, *Tectonophysics*, *151*, 137–165, 1988.

Shimizu, N., The geochemistry of olivine-hosted melt inclusions in a FAMOUS basalt ALV519-4-1, *Phys. Earth Planet. Inter.*, *107*, 183–201, 1998.

Shimizu, N., and S. R. Hart, Application of the ion microprobe to geochemistry and cosmochemistry, *Annu. Rev. Earth Planet. Sci.*, *10*, 483–526, 1982.

Shimizu, N., and D. Hassler, Coexistaence of enriched- and depleted- MORB melts as olivine-hosted inclusions in single FAMOUS lavas, *Eos Trans. AGU, 74* (43), Fall Meet. Suppl., 644, 1993.

Show, D. M., Trace element fractionation during anatexis, *Geochim. Cosmochim. Acta*, *34*, 237–243, 1970.

Sinton, J. M., and R. S. Detrick, Mid-ocean magma chambers, *J. Geophys. Res.*, *97*, 197–216, 1992.

Smewing, J. D., Mixing characteristics and compositional differences in mantle-derived melts beneath spreading axes: Evience from cyclically layered rocks in the ophiolite of north Oman, *J. Geophys. Res.*, *86*, 2645–2659, 1981.

Sobolev, A., Melt inclusions in minerals as a source of principle petrological information, *Petrology*, *4*, 228–239, 1996.

Sobolev, A. V., and N. Shimizu, Ultra-depleted primary melt included in an olivine from the Mid-Atlantic Ridge, *Nature*, *363*, 151–154, 1993.

Solomon, M., Counting and sampling error in modal analysis by point counter, *J. Petrol.*, *4*, 367–382, 1963.

Sparks, D., and E. Parmentier, Melt extraction from the mantle beneath mid-ocean ridges, *Earth Planet. Sci. Lett.*, *105*, 368–377, 1991.

Spiegelman, M., Physics of melt extraction: Theory, implications and applications, *Philos. Trans. R. Soc. Landon, Ser. A*, *342*, 23–41, 1993.

Spiegelman, M., P. B. Kelemen, and E. Aharonov, Causes and consequences of flow organization during melt transport: The reaction infiltration instability in compactible media, *J. Geophys. Res.*, *106*, 2061–2077, 2001.

Tilton, G., C. Hopson, and J. Wright, Uranium-lead isotopic ages of the Samail ophiolite, *J. Geophys. Res.*, *86*, 2763–2775, 1981.

Van Orman, J. A., N. Shimizu, and T. L. Grove, Rare earth element diffusion in diopside and disequilibrium melting in the mantle, *Eos Trans. AGU, 79*(45), Spring Meet. Suppl., S371, 1998.